



Review

# A Review on Non-Noble Metal Substrates for Surface-Enhanced Raman Scattering Detection

Ying Chen, Yuling Hu \*  and Gongke Li 

School of Chemistry, Sun Yat-sen University, Guangzhou 510006, China; chen2268@mail2.sysu.edu.cn (Y.C.); cesgkl@mail.sysu.edu.cn (G.L.)

\* Correspondence: ceshyl@mail.sysu.edu.cn

**Abstract:** Surface-enhanced Raman scattering (SERS), a powerful spectroscopic technique owing to its abundant vibrational fingerprints, has been widely employed for the assay of analytes. It is generally considered that one of the critical factors determining the SERS performance is the property of the substrate materials. Apart from noble metal substrates, non-noble metal nanostructured materials, as emerging new substrates, have been extensively studied for SERS research by virtue of their superior biocompatibility, good chemical stability, outstanding selectivity, and unique physicochemical properties such as adjustable band structure and carrier concentration. Herein, in this review, we summarized the research on the analytical application of non-noble metal SERS substrates from three aspects. Firstly, we started with an introduction to the possible enhancement mechanism of non-noble metal substrates. Then, as a guideline for substrates design, several main types of materials, including carbon nanomaterials, transition metal dichalcogenides (TMDs), metal oxides, metal-organic frameworks (MOFs), transition metal carbides and nitrides (MXenes), and conjugated polymers were discussed. Finally, we especially emphasized their analytical application, such as the detection of pollutants and biomarkers. Moreover, the challenges and attractive research prospects of non-noble metal SERS substrates in practical application were proposed. This work may arouse more awareness of the practical application of the non-noble metal material-based SERS substrates, especially for bioanalysis.

**Keywords:** surface-enhanced Raman scattering; detection; non-noble metal nanomaterials substrate



**Citation:** Chen, Y.; Hu, Y.; Li, G. A Review on Non-Noble Metal Substrates for Surface-Enhanced Raman Scattering Detection. *Chemosensors* **2023**, *11*, 427. <https://doi.org/10.3390/chemosensors11080427>

Academic Editor: Barbara Palys

Received: 28 June 2023

Revised: 21 July 2023

Accepted: 27 July 2023

Published: 1 August 2023



**Copyright:** © 2023 by the authors. Licensee MDPI, Basel, Switzerland. This article is an open access article distributed under the terms and conditions of the Creative Commons Attribution (CC BY) license (<https://creativecommons.org/licenses/by/4.0/>).

## 1. Introduction

Surface-enhanced Raman scattering (SERS) has become an ideal approach for the real-time detection of various samples due to the advantages of unique fingerprint identification, no sample pretreatment, rapid detection, and low reagent consumption [1–4]. In fact, of the various factors that affect SERS performance, the design and fabrication of high-performance SERS substrates are the most critical to promoting the development of SERS technology. Traditionally, noble metal nanomaterials of different shapes and sizes have always been employed as SERS substrates, which can induce prominent localized surface plasmon resonance (LSPR) under electromagnetic radiation, generating huge electromagnetic field nearby, thereby drastically enhancing Raman signals of target molecules to achieve ultra-high SERS sensitivity [5,6]. As a promising complement to noble metal substrates, the introduction of non-noble metal nanostructures has injected new vitality into the traditional SERS and is of great significance for expanding the application of SERS.

So far, various non-noble metal nanomaterials with the advantages of high uniformity, good chemical stability, and significant biocompatibility have been widely studied as SERS substrates [7,8]. Compared to noble metal SERS substrates, they can not only achieve efficient electromagnetic enhancement (EM) with a low damping rate and reduced Ohmic loss [9–11] but also could adjust the charge transfer to achieve enhanced Raman scattering [12]. Moreover, recent studies have also shown that chemical enhancement

(CM) usually coexisted with EM in non-noble metal substrates, which indicated that the substrates effectively combined with the two mechanisms were expected to achieve highly sensitive SERS detection [13–15]. As a unique characteristic of non-noble metal nanomaterials, it can hinder the combination of electrons and holes by effectively transferring free electrons. Thus, the fluorescence background of probe molecules was destroyed, further improving the resolution of SERS detection [16,17]. Moreover, the high selectivity owing to the CM effect of non-noble metal SERS substrates can distinguish specific molecules from complex environments [18,19]. Based on this, non-noble metal nanomaterials, as the promising candidate nanomaterials for SERS substrates, show a huge application prospect in SERS detection. However, most reviews regarding non-noble metal SERS substrates are focused on the summary of the material engineering, such as the category of substrates and approaches to boost SERS performance, including morphology design, size adjustment, defect engineering, crystallinity, and phase structure [10,12]. In fact, non-noble metal SERS substrates also have practical application potential in many fields, but this aspect is often ignored.

In this review, we concentrate on the latest application progress of SERS active non-noble metal nanomaterials, as presented in Figure 1. Firstly, the enhancement mechanism of non-noble metal materials was discussed briefly. Subsequently, several main types of non-noble metal materials were introduced. Finally, as an important part of the review, various promising applications of non-noble metal SERS substrates for the detection of pollutants and biomarkers were summarized. Moreover, we proposed current challenges and future perspectives of non-noble SERS substrates in practical detection with a view to maximizing their great potential.

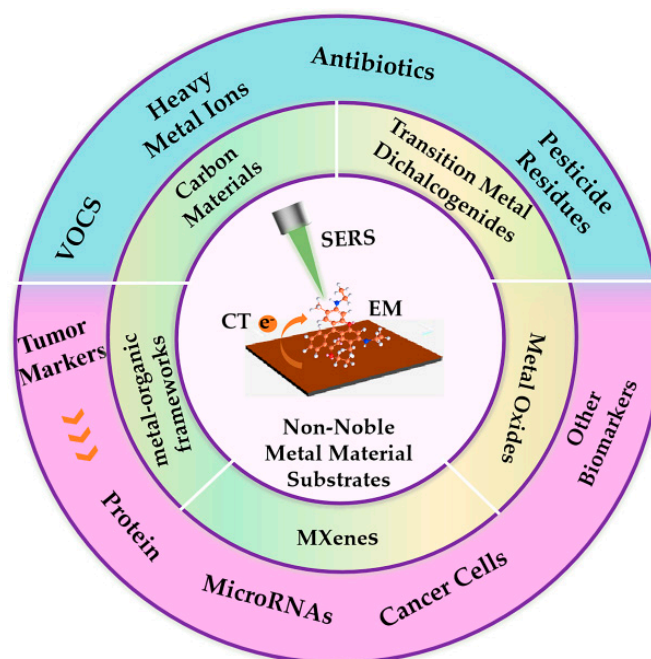


**Figure 1.** Overview of non-noble metal nanomaterials employed in SERS detection.

## 2. Raman Enhancement Mechanism of Non-Noble Metal SERS Substrates

Due to the wide variation in material preparation and properties, the mechanism of non-noble metal SERS substrates is relatively complex. According to the existing research results, the two key mechanisms that are widely accepted for describing the SERS enhancement effect include EM and CM [20,21].

EM is generally believed to result from the enhancement of local electromagnetic field generation by the collective oscillations of plasma nanoparticles or rough surfaces with surface roughness ranging from tens to hundreds of nanometers due to surface plasmon resonance (SPR) [9,22,23]. For most non-noble metal nanomaterials, the surface plasma

frequency ( $\omega_{sp}$ ) rises in proportion to the electron density [24,25]. However, the electron density is presumed to be small in the conduction band of them. Thus, it is often stated that  $\omega_{sp}$  lies in the infrared. Fortunately, the bandgap and carrier concentration of most non-precious metals is adjustable, resulting in an LSPR effect in the visible region. Meanwhile, Mie scattering can enhance the electric field in non-noble metal micro- or nanostructures at certain diameters. When the molecules adhered to the surface of non-noble metal materials satisfy the excitation conditions of Mie resonance, the generated electric near-field significantly enhances the coupling between the incident wave and the molecules, thereby enhancing the Raman signal of the absorbed molecules [24–26]. Compared to EM, CM mainly relies on the amplification of the Raman polarization tensor by chemical adsorption of molecules on the surface of non-noble metal nanomaterials and plays a more critical role in the Raman enhancement of non-noble metal SERS substrates. For the molecular-non-noble metal nanomaterial system, the enhancement of CM mainly comes from charge transfer (CT), which depends on the energy levels between a molecule and the substrate, which results in the enhanced selectivity of the substrates towards the molecules [27,28]. When the CT occurred between the molecule and the substrate material, the molecular polarizability and electron density distribution changed, resulting in the SERS effect [29].

In order to further improve the SERS performance of non-noble metal substrates, a “coupled resonance” effect was proposed. It requires that the selection of the substrates-molecule system and relevant experimental parameters must conform to the SERS rules of producing synergistic resonance effects, including molecular resonance, substrates-molecular CT resonance, and exciton resonance [30]. It is worth mentioning that exciton resonance is also a unique electronic property of most non-noble metal materials, and the SERS performance is also improved when the frequency of the incident light is close to the exciton resonance frequency.

### 3. Classification of Non-Noble Metal SERS Substrates

As promising complements to the current most popular plasmonic metal SERS substrates, non-noble metal materials have attracted more and more researchers to engage in the SERS field due to their many appealing attributes. Firstly, we classified and summarized non-noble metal SERS substrates, including carbon nanomaterials, transition metal dichalcogenides (TMDs), metal oxides, metal-organic frameworks (MOFs), transition metal carbides and nitrides (MXenes), and conjugated polymers.

#### 3.1. Carbon Materials-Based SERS Substrates

Carbon materials have been widely employed as the SERS active substrates due to their excellent surface uniformity and enhancement efficiency [31]. Graphene, as a typical carbon material, is prone to coupling with biomolecules and aromatic chemicals due to the presence of a large delocalized  $\pi$  bond and shows obvious merits as a SERS substrate [32]. Ling et al. [33] first reported the SERS phenomenon on graphene surfaces using phthalocyanine (Pc), rhodamine 6G (R6G), protoporphyrin IX (PPP), and crystal violet (CV) as probe molecules in 2010 (Figure 2). Researchers have fabricated graphene with higher SERS activity by doping or forming heterojunctions. For example, Feng et al. [34] prepared nitrogen-doped graphene as a SERS substrate and confirmed that this substrate had a lower SERS detection limit than graphene. Ghopry et al. [35] reported a graphene heterostructure SERS substrate with high sensitivity. The detection range of R6G obtained on the substrate is  $5 \times 10^{-11} \sim 5 \times 10^{-12}$  M. In addition to graphene, its oxidized derivatives, such as graphene oxide (GO), can also be used as SERS substrates. Singh et al. [36] used GO and RGO sheets with large areas as SERS substrates for the detection of rhodamine B. The result exhibited a high EF of  $10^4$  and a low detection limit of 10 nM.

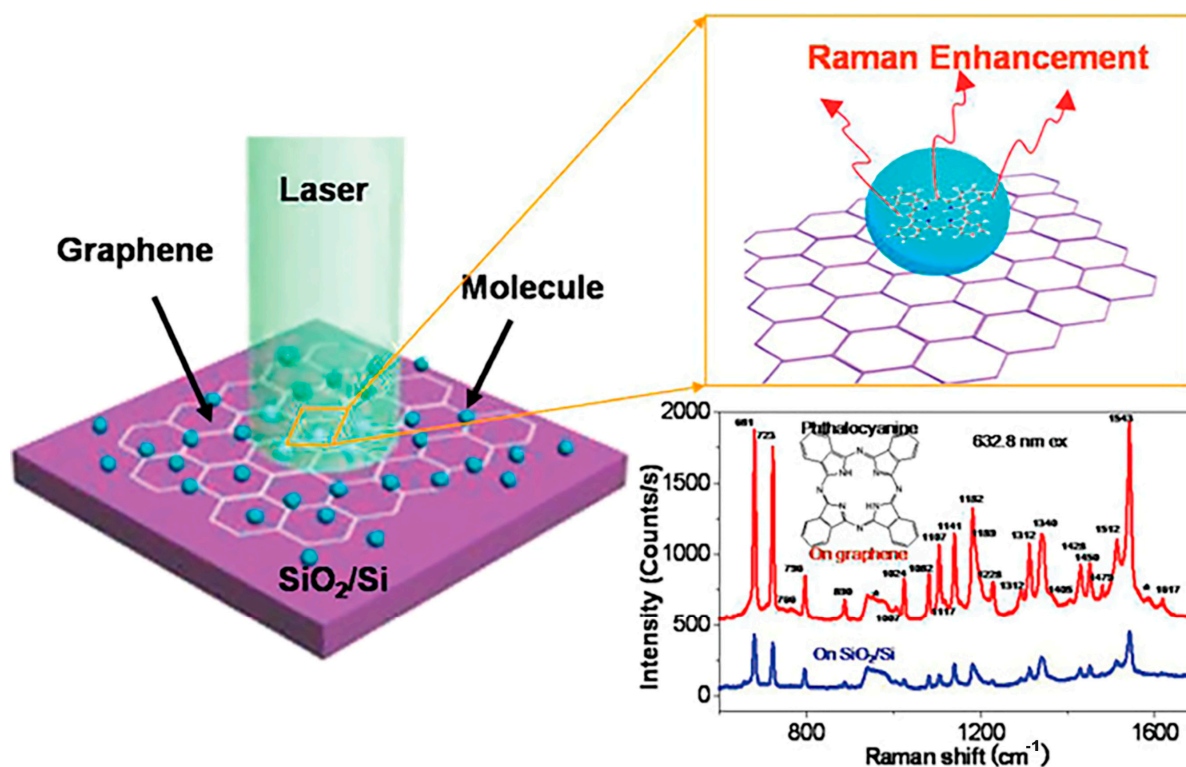


**Figure 2.** Schematic illustration of the molecule on graphene and a SiO<sub>2</sub>/Si substrate, and the comparison of Raman signals of phthalocyanine deposited on graphene (red line) and on the SiO<sub>2</sub>/Si substrate (blue line) at 632.8 nm excitation. Reprinted with permission from [33]. Copyright 2010 American Chemical Society.

### 3.2. TMDs-Based SERS Substrates

TMDs can be represented by a general formula MX<sub>2</sub>, in which M is a transition metal atom (group III B–VIII), and X is a chalcogen atom (S, Se, Te). It has tunable optical and electronic properties, resulting in many excellent photoelectric properties, including SERS [37,38]. Molybdenum disulfide (MoS<sub>2</sub>) is the most typical material in TMDs. It was also the first TMDs with SERS activity found by Ling et al. [39]. However, its enhancement effect was low. Therefore, researchers have proposed different strategies to improve the SERS performance of MoS<sub>2</sub>. Considering the layer-dependent effect of two-dimensional (2D) MoS<sub>2</sub>, Lee et al. [40] demonstrated that the monolayer MoS<sub>2</sub> produced the most obvious Raman enhancement than 3 L and bulk MoS<sub>2</sub>. Moreover, Li et al. [41] achieved efficient CT from MoS<sub>2</sub> to probe molecules by adjusting the interlayer distance of MoS<sub>2</sub> and obtained an EF as high as  $5.31 \times 10^5$  (Figure 3). Majee et al. [42] prepared interconnected and vertically oriented few-layer MoS<sub>2</sub> nanosheets (NTNs) as an ultrasensitive SERS substrate by adjusting the growth arrangement mode of MoS<sub>2</sub>. In addition to the above methods, other methods, including defect/active site induction [43], chemical doping [44], and heterostructure design [45], are also useful in improving the SERS performance of MoS<sub>2</sub>. The study of MoS<sub>2</sub> SERS activity has opened the way to study the SERS enhancement of TMDs. Subsequently, a series of TMDs with complex band structures and rich electronic states have been explored, such as SnS<sub>2</sub>, MoTe<sub>2</sub>, NbTe<sub>2</sub>, and so on [46–48].



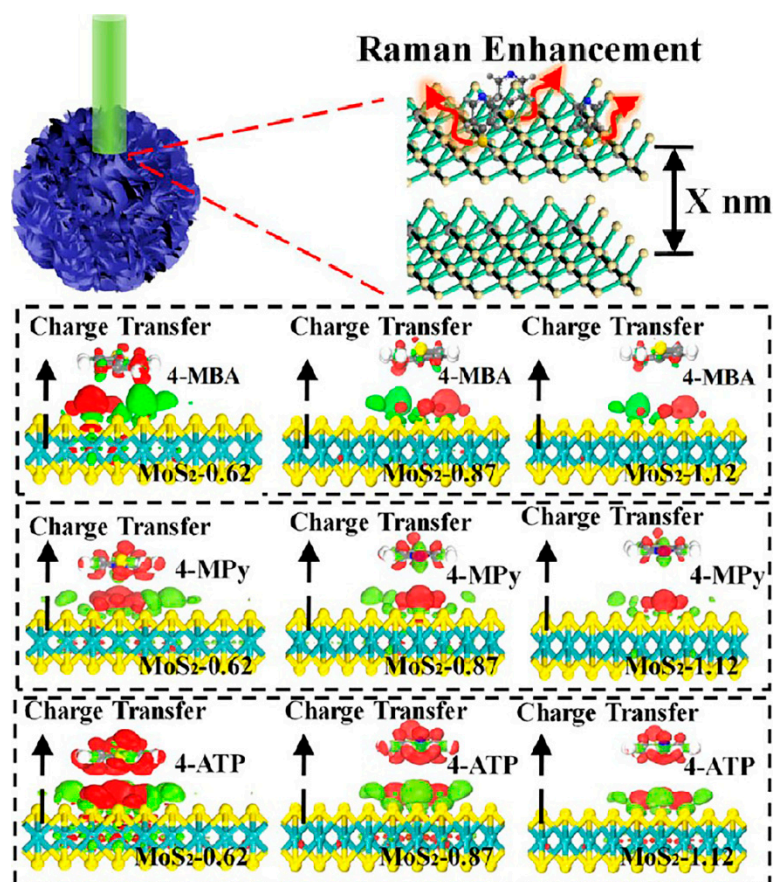


**Figure 3.** Scheme of the Raman enhancement and difference of total electron density distributions between MoS<sub>2</sub>-0.62 (MoS<sub>2</sub>-0.87 or MoS<sub>2</sub>-1.12) and 4-MBA/4-MPy/4-ATP. The red (green) distribution stands for electron accumulation (depletion). Reprinted with permission from [41]. Copyright 2014 American Chemical Society.

### 3.3. Metal Oxide-Based Substrates

The promising properties such as physio-chemical stability, high uniformity, high refractive index, and tunable band gap of metal oxide make them excellent SERS substrates [49]. As early as 1982, Yamada et al. observed the SERS effect on the surface of NiO and TiO<sub>2</sub> [50,51]. With the continuous gushing of metal oxides, it was proved that many metal oxide materials exhibit SERS activity, including ZnO, Fe<sub>3</sub>O<sub>4</sub>, Cu<sub>2</sub>O, MoO<sub>2</sub>, WO<sub>3</sub>, VO<sub>2</sub>, Nb<sub>2</sub>O<sub>5</sub>, Ta<sub>2</sub>O<sub>5</sub>, Ti<sub>3</sub>O<sub>5</sub>, etc. [10]. Among them, MoO<sub>2</sub> is considered to be an ideal material for SERS substrate because it has a large number of free electrons, which can lead to the formation of the LSPR effect [52]. Wu et al. [53] synthesized ultrathin MoO<sub>2</sub> nanosheets (NTNs) as a SERS substrate; they demonstrated that the substrate has superior signal uniformity in the whole area with a limit of detectable concentration down to  $4 \times 10^{-8}$  M and EF up to  $2.1 \times 10^5$ . Moreover, Miao et al. [54] revealed enhanced SERS signals of probe molecules on defect-rich VO<sub>2</sub> NTNs. Moreover, Li et al. [55] obtained novel quasi-metallic  $\gamma$ -Ti<sub>3</sub>O<sub>5</sub> with a strong LSPR effect by reducing TiO<sub>2</sub> microspheres and using it as a SERS substrate. The results showed that the reduced  $\gamma$ -Ti<sub>3</sub>O<sub>5</sub> showed a 10,000-times increase in SERS sensitivity compared to TiO<sub>2</sub> microspheres, and the lowest detectable limit is up to  $10^{-10}$  M (Figure 4). In fact, in addition to fabricating novel metal oxide substrates with high SERS activity, it is also an effective strategy to explore their enhancement mechanism to improve their sensitivity. The crystallinity of metal oxides can affect SERS performance by adjusting the CT process. Compared with crystalline metal oxides, amorphous structures are more conducive to the electron transfer process [10,56]. This could be ascribed to the fact that amorphous structures can reduce electron confinement, improve light scattering (such as ZnO nanocages), or enhance molecular adsorption

(such as  $\text{MoO}_{3-x}$  quantum dots). In addition, the SERS substrates of sub-stoichiometric metal oxides have rich defect electronic states associated with surface oxygen vacancies, which can synergistically enhance excitons and CT resonance, providing new and efficient charge escape, thus improving SERS sensitivity [57,58].

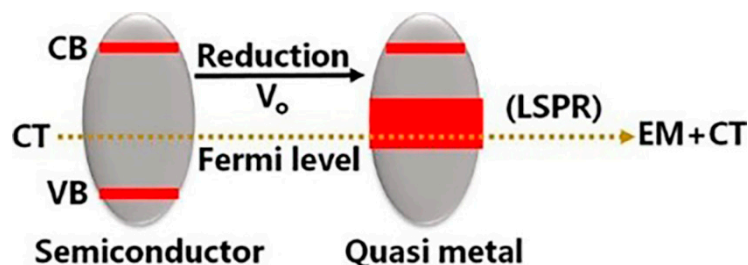


**Figure 4.** By introducing oxygen vacancies,  $\text{TiO}_2$  semiconductors with wide-band gaps are transformed into quasi-metals  $\gamma\text{-Ti}_3\text{O}_5$  with rich free electrons. Reprinted with permission from [55]. Copyright 2019 American Chemical Society.

### 3.4. MOFs-Based Substrates

MOFs are a new class of hybrid organic-inorganic supramolecular materials that have a large surface area, porous properties, chemical stability, and uniform and tunable nanostructured cavities, which strongly favor potential use as a substrate [59–61]. Although the SERS phenomenon based on noble metals and MOF hybrids has been discussed [62–64], MOF materials are generally regarded as a template to load tightly ordered and well-dispersed SERS-active NPs, and it is believed that the SERS enhancement resulted from the contributions of noble metal particles. Until Yu et al. [65] reported the SERS enhancement phenomenon of methyl orange molecule on the surface of MOFs in 2013 (MIL-100 and MIL-101), thereafter, with the continuous exploration of MOF materials, the exploration of their SERS activity also received attention. Sun et al. [66] achieved the transformation of MOF materials from non-SERS active substrates to SERS active substrates by careful modulation of metal centers, organic ligands, and framework topologies and obtained an EF of up to  $10^6$  (Figure 5). Moreover, Fu et al. [67] reported MIL-100 (Fe) as a SERS substrate with high SERS activity.

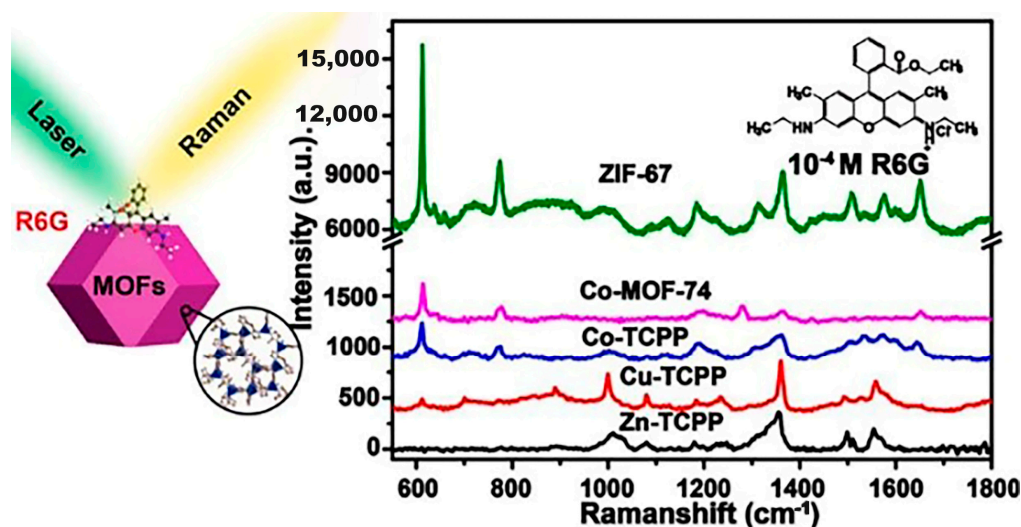


**Figure 5.** Schematic illustration of the molecule on MOFs substrate and the comparison of Raman signals of R6G deposited on Co-MOF-74 and on the TCPP-based MOF compounds with different metal ions. Reprinted with permission from [66]. Copyright 2018 American Chemical Society.

### 3.5. MXene-Based Substrates

MXenes, composed of transition metal carbides/nitrides, is a kind of semi-metal material with high electric conductivity and has the ability to generate plasmon resonance in the visible or near-infrared range. These unparalleled properties render them promising candidates for SERS substrates [32,68,69]. Sarycheva et al. [69] first demonstrated that 2D  $\text{Ti}_3\text{C}_2\text{T}_x$  MXene as a SERS substrate exhibited good SERS activity with an EF of up to  $10^6$ . An important potential advantage of MXenes is the ability to deposit materials on different substrates, including flexible materials. Soundiraraju et al. [70] prepared different SERS substrates based on paper, silicon, and glass by loading  $\text{Ti}_2\text{NT}_x$  onto them. The results showed that  $\text{Ti}_2\text{NT}_x$  had the highest enhancement efficiency up to  $10^{12}$  on paper-based substrates (Figure 6). In addition, Yang et al. [71] introduced ultraflexible characteristics of  $\text{Ti}_3\text{C}_2\text{T}_x$  MXene into SERS microfluidic chips, which significantly improved the detection sensitivity of SERS microfluidic sensors. Although the development of MXene-based substrates is still in the first stages, according to the current reported results, MXene materials will become promising novel SERS substrates.

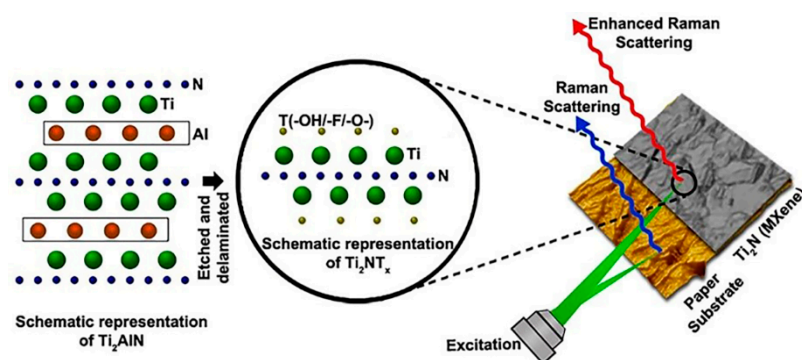


**Figure 6.** Illustration of the preparation of  $\text{Ti}_2\text{NT}_x$  and the detection of analysis. Reprinted with permission from [70]. Copyright 2017 American Chemical Society.

### 3.6. Conjugated Polymers-Based Substrates

Conjugated polymers are organic macromolecules that have attractive optical properties due to the delocalized  $\pi$  electron cloud on their main chain [27,72]. It is considered a promising new type of non-noble metal SERS substrate. Among them, covalent organic frameworks (COFs), as a newly emerging material of conjugated polymer, have been widely concerned by researchers in the SERS field due to their high specific surface area, excellent thermal stability, and abundant surface functional groups [73,74]. In particular, small molecule screening can be realized based on the synergistic effect of pore and surface functional groups of COFs materials. It was helpful to improve the selectivity of SERS detection. Nevertheless, the Raman enhancement ability of COFs substrates is much lower than inorganic and noble metal SERS substrates. At present, in order to gain a high analytical sensitivity, metal-COFs composites were introduced into SERS-based assays.

## 4. Non-Noble Metal Materials for Analytical Application

Non-noble metal nanomaterials have recently been widely used as SERS substrates in various fields due to their particular advantages. For example, they have abundant surface sites that are different from noble metal materials, which provide a large number of coordination sites for the modification and functionalization of other molecules. Meanwhile, the combination of the two can further improve the stability of the modified molecules on the non-noble metal materials surface. In addition, non-noble metal materials can also be used as flexible substrates, which makes it possible to in situ detect pesticide residues on the surface of fruits and vegetables. The good biocompatibility of non-noble metal substrates especially makes them produce great breakthroughs in bioimaging, cancer diagnosis, and treatment [75–77]. It should be mentioned that the unique catalytic properties of non-noble metal materials also enable the development of renewable materials. Herein, in this section,

we will give a detailed introduction to the recent application of non-noble metal materials as SERS substrates in different fields.

#### 4.1. Detection of Pollutants

The increase in pollutants such as volatile organic compounds (VOCs), heavy metal ions, and antibiotics every year has created an enormous burden threatening ecological cycles and public health. Thus, the detection of them was given high priority. SERS, as a universal analytical technique, has been considered a label-free and ultra-sensitive detection tool for the detection of a wide range of adsorbent molecules [78–80]. As SERS substrates with important and promising at present, non-noble metal nanomaterials have the advantages of being environmentally friendly, non-energy intensive, nontoxic, and cost-friendly, and have wide application prospects in pollutant detection. Some of these non-noble metal SERS substrates have a large surface area, which can achieve high enrichment of heavy metal ions and gases, thus improving their detection sensitivity. In addition, the inter-band-gap states electrons of non-noble metal substrates with band gaps can promote the reduction of the redox potential of the ions couple, resulting in the change of valence states of heavy metal ions so as to achieve the selective detection of them.

##### 4.1.1. Detection of VOCs

Yang et al. [71] prepared SERS substrate by adhering ultraflexible  $\text{Ti}_3\text{C}_2\text{T}_x$  MXene onto the surface of three-dimensional (3D) honeycomb arrays and introduced them into microfluidic chips (Figure 7a).  $\text{Ti}_3\text{C}_2\text{T}_x$  MXene has a universal high adsorption efficiency of various gases, and its super flexible well retained the sophisticated nanomicrostructure that generated the vortex fields to extend the molecule residence time and kept the analytes inside the SERS-active hot spots, leading to the increased sensitivity. Thus, three typical VOCs with different functional groups, including 2, 4-dinitrotoluene (DNT), and benzaldehyde and indole, can be achieved by the SERS-vortexene chip with high repeatability. The LODs for DNT, benzaldehyde, and indole were about 10, 10, and 50 ppb, respectively.

##### 4.1.2. Detection of Heavy Metal Ions

Lead, arsenic, mercury, and other heavy metals are not only the most toxic contaminants but they are considered human carcinogens [81,82]. In order to effectively monitor the above-mentioned heavy metal pollutants, a great deal of work based on SERS detection has been reported. For example, Zhang et al. [83] prepared ZnO submicron flowers (ZnO SFs) as a substrate for sensitive detection of  $\text{Pb}^{2+}$ . The ZnO SFs substrate exhibited a narrower energy band, which promoted the coupling resonance of the molecular-substrate system, thus improving the CT efficiency and achieving a significant SERS enhancement effect. Furthermore, by utilizing the free-legged DNA walker amplification strategy, an ultrasensitive biosensor was constructed to monitor  $\text{Pb}^{2+}$ . The experimental data demonstrated that this biosensor could efficiently determine  $\text{Pb}^{2+}$  with a low detection of 3.55 pM. Similarly, Parveen et al. [84] used ZnO nanoparticles (NPs) functionalized single-wall carbon nanotubes (SWCNTs) as a nanocomposite SERS sensor for the detection of  $\text{Pb}^{2+}$  ions in an aqueous medium. The prepared sensor exhibited high selectivity and low limit of detection for  $\text{Pb}^{2+}$  ions (0.225 nM). In addition, a dye-sensitized non-noble metal colloid system can also show synergistic effects in the detection of metal ions. Ji et al. [85] reported an example of using alizarin red S (ARS) sensitized colloidal  $\text{TiO}_2$  NPs as a SERS substrate for the detection of Cr (VI) in water. In the presence of Cr (VI), the ARS molecule stably adsorbed on the surface of colloidal  $\text{TiO}_2$  NPs can achieve self-degradation, leading to the decrease of SERS signal intensity. The detection of Cr (VI) can be achieved by monitoring the SERS intensity of the ARS probe molecule. This ARS- $\text{TiO}_2$  complex could be further applied to the detection of Cr (VI) in environmental samples.



#### 4.1.3. Detection of Antibiotics

Antibiotic chemicals are not only an important source of water pollution, but also the existence of excessive antibiotics can cause the problem of antibiotic resistance, which poses a serious threat to human and animal health [86,87]. Therefore, ensuring the rational use of antibiotics and effective monitoring has always been the focus of research. Recent studies have shown that antibiotics can be effectively detected by non-noble metal SERS substrates. For example, Wang et al. [48] prepared 2D niobium ditelluride (NbTe<sub>2</sub>) nanosheets (NTNs) for the detection of ciprofloxacin (CIP) and enrofloxacin (ENR) antibiotics molecules (Figure 7b). Based on the fluorescence quenching effect of NbTe<sub>2</sub> NTNs and CT between the analytes, the ultrasensitive detection of CIP and ENR was achieved. The LODs were 35.1 and 35.9 ppb, respectively. In addition, Singh et al. [88] synthesized 3D MoS<sub>2</sub> nanoflowers (NFs) with tunable surface area (5–20 m<sup>2</sup>/g) as a SERS substrate to realize ultrafast SERS detection of various antibiotics. In particular, MoS<sub>2</sub> NFs have a narrow bandgap and high specific surface area, which significantly enhances light-harvesting and adsorption capability, leading to the improvement of their photodegradation behavior. Therefore, the photocatalytic degradation experiment-based SERS monitoring was realized. The results showed that even a very low amount (0.025 mg) of MoS<sub>2</sub> NFs (20 m<sup>2</sup>/g) can tremendously decompose oxytetracycline hydrochloride (OTC-HCl) molecules within 60 min under visible light.

#### 4.1.4. Detection of Pesticide Residues

The excessive use of pesticides has gained increasing attention in recent years owing to their enormous menace to human health. SERS is a useful ultrasensitivity detection tool, which is of great significance for the monitoring of pesticide residue levels. As excellent SERS substrates for the detection of pesticide residues, non-noble metal nanomaterials not only exhibited trace level SERS response but also could be used for in situ detection of pesticide residues on the surface of fruits and vegetables. For example, Zhang et al. [89] prepared a plasmonic MoO<sub>2</sub> nanosphere as a highly sensitive SERS substrate for the detection of various pesticides (Figure 7c). In order to verify the feasibility of this substrate in practical application, clenbuterol hydrochloride (CH), methyl parathion (MP), and 2, 4-dichlorophenoxyacetic acid (2, 4-D) were chosen as pesticide models. Experimental data indicated that this substrate could achieve the quantification of the above pesticide models with a LOD of 10<sup>-7</sup> M. Another balsam pear-shaped CuO with dense nanoparticle protuberance was reported by Liang et al. [90]. In their work, the paraquat solution was taken as an example. Attributed to the CuO substrate's unique shape and rough surface, more "hot spots" were generated on the particle surface, which significantly enhanced the SERS effect. This substrate could detect paraquat with a detection limit of 275 µg L<sup>-1</sup>. Moreover, Quan et al. [91] successfully prepared MoS<sub>2</sub>/TiO<sub>2</sub> substrate (MTi<sub>20</sub>) assembled from MoS<sub>2</sub> nanoflowers (NFs) and TiO<sub>2</sub> NPs, which exhibited ultra-high SERS response to α-endosulfan, the LOD of α-endosulfan can reach 10<sup>-8</sup> M. In addition, Gokulakrishnan et al. [92] fabricated a flexible rGO SERS active substrate for in situ detection of thiabendazole (TBZ). Owing to the large surface area, the flexible rGO SERS substrate could detect TBZ with a LOD of 1 nM. Furthermore, they further demonstrated that the flexible SERS substrates could also be used for detecting pesticides on target surfaces with complex geometries like fruits, leaves, and vegetables.

Table 1 summarizes the SERS detection results of non-noble metal substrates for various pollutants above-mentioned, such as VOCs, heavy metal ions, antibiotics, and pesticide residues.

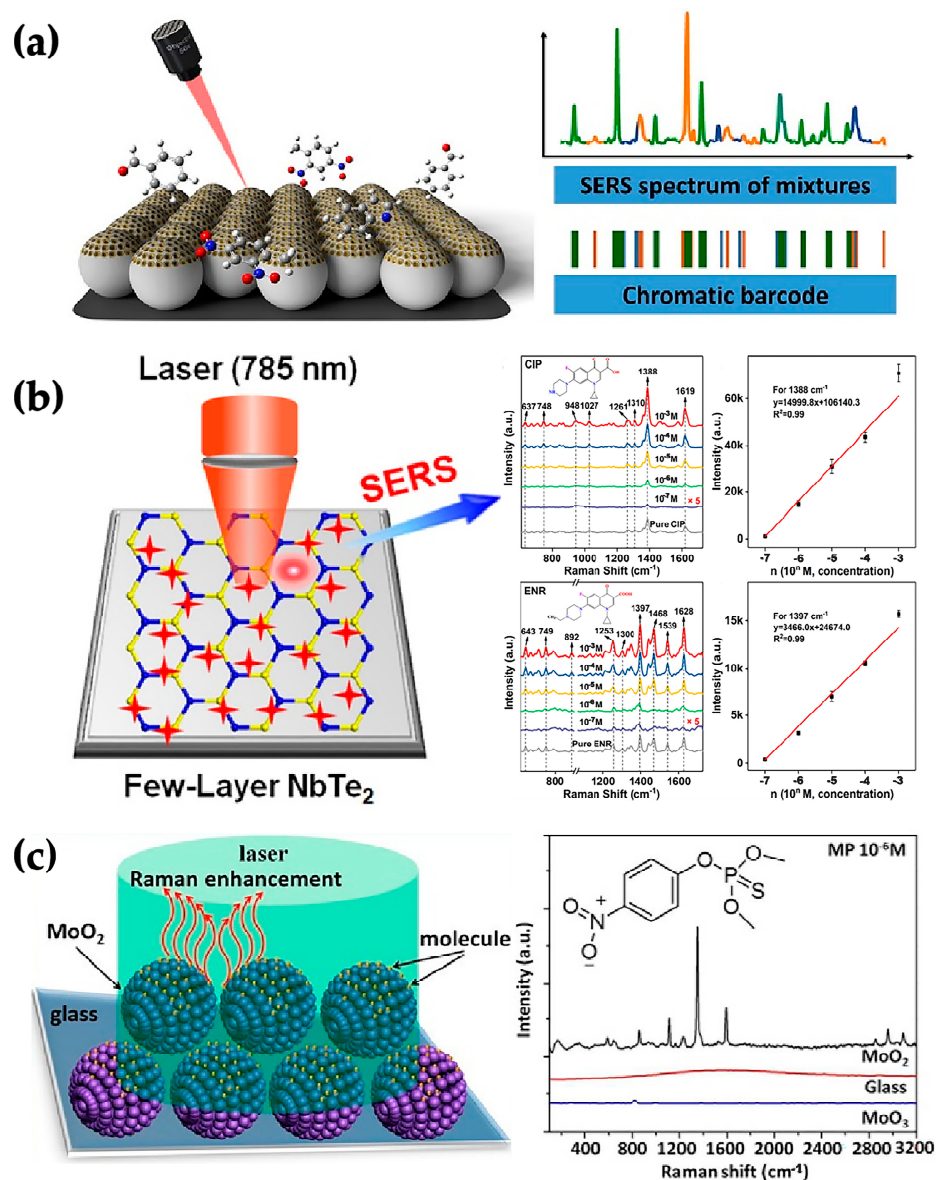


**Figure 7.** (a) Schematic diagram of multiplex VOCs mixture detection. (b) Schematic illustration of the ultrathin NbTe<sub>2</sub>-based SERS experiment and SERS measurement of ciprofloxacin and enrofloxacin antibiotics molecules adsorbed on NbTe<sub>2</sub> NTNs substrates. (c) Schematic diagram of the SERS experiment and SERS spectra of methyl parathion on the MoO<sub>2</sub> substrates. (a) Reprinted with permission from [71]. Copyright 2021 American Chemical Society. (b) Reprinted with permission from [48]. Copyright 2020 American Chemical Society. (c) Reprinted with permission from [89]. Copyright 2017 American Chemical Society.

**Table 1.** A summary of non-noble meta-based SERS substrates for pollutant detection is mentioned in this review.

SERS Substrate	Enhancement Mechanism	Target	Linear Range	LOD	Ref
Honeycomb-like 3D Ti <sub>3</sub> C <sub>2</sub> T <sub>x</sub>	Synergistic effect of strong adsorption capacity of substrate and EM	Benzaldehyde 2, 4-dinitrotoluene indole	/	10 ppb 10 ppb 50 ppb	[71]
ZnO SFs	Synergistic effect of CT and Mie resonance enhancement	Pb <sup>2+</sup>	10 pM–100 μM	3.55 pM	[83]

Table 1. Cont.

SERS Substrate	Enhancement Mechanism	Target	Linear Range	LOD	Ref
ZnO@SWCNTs	Synergistic effect of “hot spot” generated by intertube and interparticle coupling, as well as CT enhancement	Pb <sup>2+</sup>	0.01–100 μM	0.225 nM	[84]
ARS-TiO <sub>2</sub> complexes	CT enhancement	Cr (VI)	0.6–10 mM	0.6 mM	[85]
NbTe <sub>2</sub> NTNs	Synergistic effect of CT enhancement and fluorescence quenching effect of substrate	Ciprofloxacin enrofloxacin	351 ppm–35.1 ppb	35.1 ppb 35.9 ppb	[48]
3D-MoS <sub>2</sub> NFs	Synergistic effect of effective enrichment capability of substrate and CT enhancement	Oxytetracycline hydrochloride	/	/	[88]
MoO <sub>2</sub> nanospheres	LSPR effect in the visible and near-infrared (NIR) range	Clenbuterol hydrochloride methyl parathion 2,4- dichlorophenoxyacetic acid	10 <sup>-7</sup> –10 <sup>-4</sup> M	10 <sup>-7</sup> M	[89]
Balsam pear-shaped CuO	Synergistic effect of EM and CT enhancement	Paraquat	10 <sup>-7</sup> –10 <sup>-3</sup> M	10 <sup>-7</sup> M	[90]
MTi <sub>20</sub>	Interfacial CT enhancement	α-endosulfan	10 <sup>-8</sup> –10 <sup>-4</sup> M	10 <sup>-8</sup> M	[91]
Flexible rGO	Synergistic effect of effective enrichment of substrate and CT enhancement	Thiabendazole	10 <sup>-9</sup> –10 <sup>-3</sup> M	10 <sup>-9</sup> M	[92]

#### 4.2. Detection of Biomarkers

Currently, cancer remains one of the most serious health problems in the world and the leading cause of death [93,94]. Therefore, the realization of cancer screening is particularly important, which can help find early cancers and improve survival. Among the many detection techniques, SERS is a trace detection technique with a unique fingerprint spectrum, and its application can even be extended to a single molecule detection level. As a good candidate for studying and simulating biological reactions, non-noble metal SERS substrates can not only serve as a potential interface for immobilizing biomolecules but also maintain their biological activity. In this way, tumor markers, including protein, nucleic acid, and circulating tumor cells (CTCs), can be monitored by non-noble metals SERS substrates to achieve early screening of cancers.

##### 4.2.1. Detection of Protein Tumor Markers

As an example of carbohydrate antigen 19-9 (CA19-9), which has been a widely used clinical protein marker of cancer in human serum, Jiang et al. [16] designed a SERS-based immunoassay mediated by MoS<sub>2</sub> for the sensitive and specific monitoring of carbohydrate antigen CA19-9. In their work, the corresponding antibodies absorbed on the MoS<sub>2</sub> NTNs and MoS<sub>2</sub> NFs modified by the probe molecule R6G, respectively. Thus, a sandwich immunostructure was constructed by the specific recognition of anti-CA19-9 and target CA19-9. The concentration of target CA19-9 was indirectly reflected by the intensity variation of the SERS signal of R6G. The sandwich immunostructure could detect target CA19-9 with a LOD of  $3.43 \times 10^{-4}$  IU·mL<sup>-1</sup>. Furthermore, it could also be used for target CA19-9 detection in several clinical patient serum samples, which had higher sensitivity compared with the conventional chemiluminescent immunoassay (CLIA) strategy. Using a similar principle of specific recognition, Liu et al. [95] designed methylene blue (MB) modified aptamer attached to the tungsten trioxide (WO<sub>3</sub>) film for the SERS detection of glioblastoma biomarkers vascular endothelial growth factor (VEGF) in human serum

samples. In their work, MB-modified aptamer serves as a SERS signal source. After the aptamer specifically linked to VEGF, it folded into a conformationally restricted stem-loop structure, forcing the MB molecule to contact the substrate, which leads to a significant enhancement of SERS signals, thus achieving sensitive detection of VEGF. The proposed aptasensor could detect VEGF with high selectivity, while the detection limit was down to  $8.7 \text{ pg}\cdot\text{mL}^{-1}$ .

#### 4.2.2. Detection of MicroRNAs

MicroRNAs (miRNA) is a noncoding single-stranded RNA molecule with approximately 18–25 nucleotides and has been verified as promising biomarkers for cancer diagnosis [96,97]. For example, Jiang et al. [98] developed a 3D  $\text{WO}_3$  hollow microsphere as a SERS-active substrate for miRNA 155 detection (Figure 8a). The 3D  $\text{WO}_3$  hollow microsphere with a small band gap and rich surface defects promoted an increase in CT, resulting in a large SERS enhancement. Then, by employing a catalytic hairpin assembly (CHA) strategy, a SERS biosensor based on a 3D  $\text{WO}_3$  hollow microsphere was constructed for the sensitive detection of miRNA 155 with a LOD of 0.18 fM. In order to verify the feasibility of this biosensor, miRNA 155 from HeLa (cervical cancer cells) and MDA-MB-231 (human breast cancer cells) were chosen as models. Experimental data proved that this biosensor could achieve the detection of miRNA 155 in actual samples. Similar to the above miRNA 155 detection, Liu et al. [99] developed a multifunctional SERS platform composed of hexagonal boron nitride nanosheets (h-BNNS), HG DNA oligonucleotide, and copper(II) phthalocyanine (CuPc) ( $\text{CuPc@HG@BN}$ ) for the detection of miR-21. Benefiting from the circle amplification of miRNA and the high SERS effect of hBNNS, the detection of miR-21 in live cells can be realized as low as 0.7 fM.

#### 4.2.3. Detection of Cancer Cells

Circulating tumor cells (CTCs) are shed by the primary tumor, representing the characteristics of a certain tumor and playing a central role in tumor dissemination and metastases. Therefore, their detection and analysis can be very valuable in the early diagnosis of cancer [100,101]. Recently, Xu et al. [102] reported a  $\text{TiO}_2$ -based nontoxicity SERS bioprobe for CTCs detection. They used reduced bovine serum protein (rBSA) and folic acid (FA) to functionalize  $\text{TiO}_2$  NPs and used 4-mercaptobenzoic acid (4-MBA) adsorbed on the surface of  $\text{TiO}_2$  NPs as a signal molecule. Benefiting from the high targeting ability of FA towards cancer cells overexpress FR, the proposed SERS bioprobe can be effectively identified different kinds of cancer cells in rabbit blood, which has a LOD of 1 cell/mL. Due to the high efficiency of interfacial photo-induced charge transfer (PICT) and strong vibration coupling effect, the amorphous nanomaterial-molecular system has significant SERS activity. Inspired by this, Lin et al. [56] designed black  $\text{TiO}_2$  NPs (B- $\text{TiO}_2$  NPs) with crystal-amorphous core-shell structures for the precision diagnosis and treatment of cancer. The feasibility of applying the high-sensitivity SERS bioprobe based on B- $\text{TiO}_2$  NPs modified with Alizarin red (AR) signal molecule, polydopamine (PD) layer, and an antibody (AB) was verified by the detection of MCF-7 drug-resistant (MCF-7/ADR) breast cancer cells (Figure 8b). Based on of FA specific recognition and ultrahigh SERS activity of B- $\text{TiO}_2$  NPs, a novel strategy that combined microfilter CTC isolation and SERS bioprobe detection for in situ isolating and directly detecting CTCs from peripheral blood at single-cell resolution was proposed by Xu et al. [103] The SERS bioprobe was composed by Raman reporting molecule AR and FA functionalized B- $\text{TiO}_2$  NPs. Benefiting by rapid separation of microfilters and the high sensitivity of SERS spectroscopy, the SERS bioprobe of B- $\text{TiO}_2$ -AR-PEG-FA could distinguish FR-positive CTCs from peripheral blood cells efficiently within 1.5 h, and the LOD of CTCs in rabbit blood can reach to 2 cells/mL. Furthermore, this strategy has also been successfully detected in blood samples from cancer patients. In addition, Feng et al. [104] fabricated ternary heterostructure  $\text{Fe}_3\text{O}_4@\text{GO}@\text{TiO}_2$  (MGT) NC and used it to develop a robust SERS probe for the sensitive and selective detection of triple-negative breast cancer cells (TNBCs). In their work, Abs can adsorb on the surface of MGT, and the



cancer cells can be specifically captured by MGT-ABs. The introduction of CuPc molecules can reflect the SERS signals in the detection system. In this way, TNBCs models such as HCC38, MDA-MB-231, and MCF-7 detection can be monitored by the MGT-Abs-CuPc nanoprobe, and the LOD of HCC38 cell was calculated to be  $\sim 3$  cells. Different from the above studies on TiO<sub>2</sub>-based CTC SERS detection, Haldavnekar et al. [105] introduced a quantum-size 3D ZnO SERS probe for the first time in the study of labeling-free in vitro diagnosis of cancer. Due to the significant reduction of the probe size, the surface defects, such as oxygen vacancies and stacking faults, resulted in a unique exponential increase in SERS. The in vitro sensing of the 3D ZnO SERS probes was demonstrated by successfully distinguishing between cancer and non-cancer cells based on the ratio of peak intensities of lipids and proteins ( $I_{1445}/I_{1654}$ ).

#### 4.2.4. Detection of Other Biomarkers

SERS is very promising for identifying disease markers due to its unique fingerprint spectrum, high sensitivity, and large dynamic range detection [106]. To pursue more excellent biocompatibility with biological samples and spectral stability as well as reproducibility, non-noble metal substrates have been gradually applied to detect various disease markers. Huang et al. [107] implemented a signal enhancement strategy featuring graphene as a substrate for the label-free detection of key blood constituent hemoglobin (Hb) and albumin (Alb) (Figure 8c). This is the first time demonstrated that the Raman signal of biomolecules was enhanced when contacted with graphene. Similarly, Dharmalingam et al. [108] proposed the concept of atomic defect enhancement for quantum probe Raman scattering (DERS) at the molecular level detection. They significantly improved the sensitivity of DERS probes by introducing high concentrations of atomic scale defects into non-plasma quantum size probes (TiO<sub>2-x</sub>). Thus, the obtained DERS probes could be used for the label-free Raman detection of biomarkers such as ATP and EGFR peptides with low Raman cross-sections. Moreover, graphene-like nanomaterials such as MoS<sub>2</sub> have been used to detect biomolecules. Typically, Su et al. [109] successfully synthesized Ni-doped MoS<sub>2</sub> NFs (Ni-MoS<sub>2</sub> NFs) for bilirubin detection in serum. The experimental analysis results showed that the Ni-MoS<sub>2</sub> NFs SERS substrate could detect bilirubin in serum samples with a detection limit as low as  $10^{-7}$  M. In addition to the detection of biomarkers in the blood samples, Fu et al. [67] prepared an excellent SERS active substrate MIL-100 (Fe). Because of MIL-100 (Fe) unique "array sensing" characteristics, it has been successfully used for the sensitive detection of gas biomarkers of lung cancer, such as 4-ethylbenzaldehyde, acetone, and isopropanol.

Severe acute respiratory syndrome-coronavirus-2 (SARS-CoV-2) is a highly infectious virus serious that poses a serious threat to human health [110,111]. Therefore, achieving rapid, ultrasensitive, and highly reliable detection of SARS-CoV-2 in patients' bodies is of great significance for controlling the epidemic. Peng et al. [46] designed a spherical SnS<sub>2</sub> with the "nano-canyon" morphology as a SERS substrate for the detection of SARS-CoV-2 S protein and RNA to recognize and diagnose SARS-CoV-2. Benefiting from the unique nano-canyon structure, the capillary effect generated on the surface of SnS<sub>2</sub> microspheres can significantly enrich the detection molecules. At the same time, the synergistic effect of CM can achieve the EF of MB up to  $3.0 \times 10^8$  and can identify various physical forms of SARS-CoV-2 with high sensitivity. This result exhibited that the EF and LOD achieved here even much better than most reported noble metal-based SERS substrates (Table 2). In addition to the SnS<sub>2</sub> microspheres mentioned above, Peng et al. [15] also reported semi-metal material Nb<sub>2</sub>C and Ta<sub>2</sub>C MXenes with remarkable SERS enhancement as SERS substrates for SARS-CoV-2 spike protein detection. As compared with Nb<sub>2</sub>C, the Ta<sub>2</sub>C substrate had a better selective SERS-enhanced effect on molecules. Therefore, Ta<sub>2</sub>C was chosen as a model substrate for the detection of SARS-CoV-2 S protein. The detection limit of SARS-CoV-2 S protein was as low as  $5 \times 10^{-9}$  M. Similarly, Fraser et al. [47] prepared few-layered MoTe<sub>2</sub> films as a SERS substrate for  $\beta$ -sitosterol detection in a complex cell culture media. Among others, Li et al. [112] reported 2D hafnium ditelluride (HfTe<sub>2</sub>) as a new

label-free SERS substrate to detect trace uric acid, the important biomarker for gout disease, which demonstrated a reliable LOD of  $10^{-4}$  M. In addition, Sun et al. [113] proposed to use the photo-excited D-MIL-125-NH<sub>2</sub> material, which could obtain stable photo-induced oxygen vacancy (PIVO) defect as a SERS substrate for the detection of disease markers. In order to evaluate the SERS activity of the D-MIL-125-NH<sub>2</sub> substrate, dopamine was chosen as a probe molecule. It was reported that the detection of dopamine has been linked to the diagnosis of various diseases, such as Parkinson's disease [114,115]. The experimental data demonstrated that this SERS substrate could efficiently determine dopamine with a detection limit of  $6.6 \times 10^{-7}$  M, which were two orders of magnitude lower than the lowest concentrations of dopamine detected on photo-excited TiO<sub>2</sub> particles.

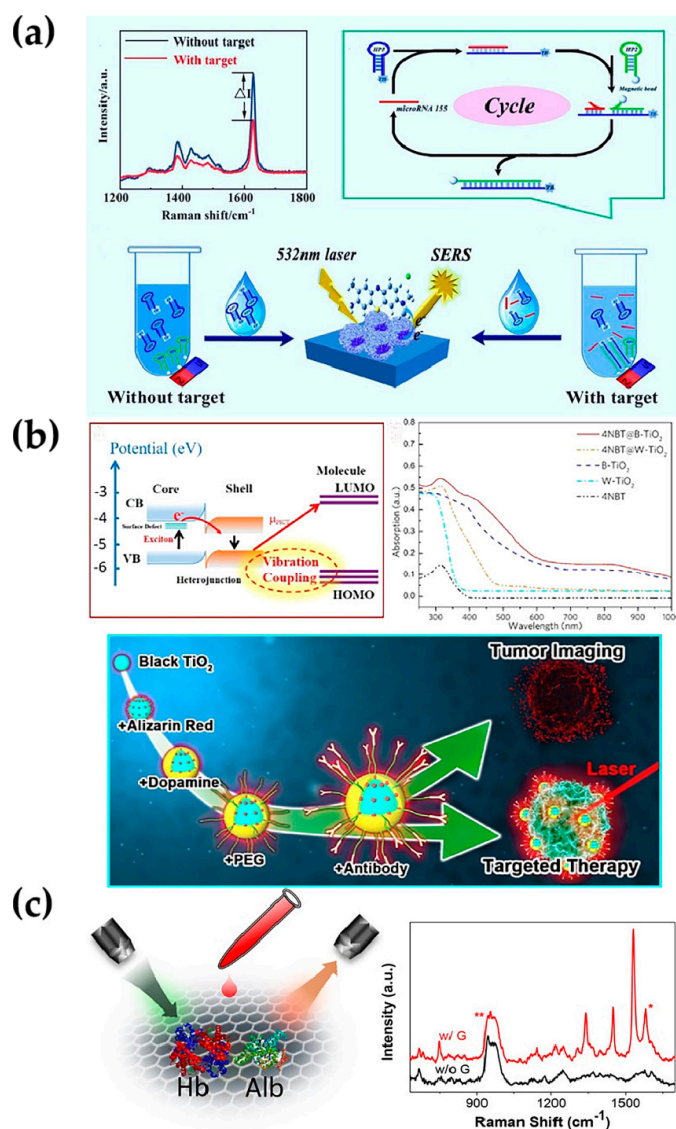


**Figure 8.** (a) Schematic diagram of the SERS Biosensor for the detection of miRNA 155. (b) Schematic diagram of the design process for B-TiO<sub>2</sub> bioprobes and their application. (c) Illustration of the GERS measurement and the Raman spectra of hemoglobin in contact with and in absence of graphene measured under 633 nm excitation laser. The graphene G bands at around  $1582\text{ cm}^{-1}$  are labeled with “\*”, and the second-order modes of Si substrate are labeled with “\*\*\*”. (a) Reprinted with permission from [98]. Copyright 2022 American Chemical Society. (b) Reprinted with permission from [56]. Copyright 2019 American Chemical Society. (c) Reprinted with permission from [107]. Copyright 2018 American Chemical Society.

**Table 2.** SERS-active substrates used for the detection of SARS-CoV-2S protein and reported SERS performance.

SERS Substrates	Target	LODs	Reported SERS Performance		Ref
			Molecules	EF	
SnS <sub>2</sub> microspheres	SARS-CoV-2S protein	10 <sup>-14</sup> M	MB	3.0 × 10 <sup>8</sup>	[46]
Ta <sub>2</sub> C		5 × 10 <sup>-9</sup> M	CV	1.4 × 10 <sup>6</sup>	[15]
Bumpy core-shell Au NPs		7.1 × 10 <sup>-16</sup> M	4-NBT	2.1 × 10 <sup>8</sup> to 2.2 × 10 <sup>9</sup>	[116]
Au/MgF <sub>2</sub> /Au		3.7 × 10 <sup>-12</sup> M	MB	2.0 × 10 <sup>5</sup>	[117]
Au NPLs/PDMS		2.6 × 10 <sup>-10</sup> M	R6G	6.4 × 10 <sup>7</sup>	[118]
Au-TiO <sub>2</sub>		10 <sup>-10</sup> M	R6G	/	[119]
Au-Ag hollow nanoshells		7.5 × 10 <sup>-15</sup> M	4-MBA	/	[120]

Table 3 summarizes the SERS detection results of non-noble metal substrates for the above-mentioned biomarkers.

**Table 3.** A summary of non-noble meta-based SERS substrates for biomarkers detection mentioned in this review.

SERS Substrate	Enhancement Mechanism	Target	Linear Range	LOD	Ref
MoS <sub>2</sub> NFs	Synergistic effect of effective enrichment of substrate and laser-induced CT resonances	CA-199	5 × 10 <sup>-4</sup> –1 × 10 <sup>2</sup> IU·mL <sup>-1</sup>	3.43 × 10 <sup>-4</sup> IU·mL <sup>-1</sup>	[16]
WO <sub>3</sub> film	CT enhancement	VEGF	10–250 pg/mL	8.7 pg/mL.	[95]
3D WO <sub>3</sub> hollow microsphere	CT enhancement	miRNA 155	1 fM–100 pM	0.18 fM	[98]
CuPc@HG@BN	Interface dipole interaction	miR-21	1.6 fM–2.8 pM	0.7 fM	[99]
TiO <sub>2</sub> -AR-rBSA-FA	Synergistic effect of strong vibration coupling resonance and PICT enhancement	SY5Y H226KYSE-150 HeLa	/	1 cell/mL	[102]
B-TiO <sub>2</sub> -AR-PD-PEG-AB	Synergistic effect of interfacial PICT and PICT resonance as well as strong vibronic coupling in amorphous shell-molecule system	MCF-7/MCF-7 drug-resistant (MCF-7/ADR) breast cancer cells	/	/	[103]
B-TiO <sub>2</sub> -AR-PEG-FA	Synergistic effect of interfacial PICT and PICT resonance as well as strong vibronic coupling in amorphous shell-molecule system	MCF-7(folate receptor (FR) positive), A549 Raw264.7 (FR negative)	1–100 cells/mL (MCF-7)	2 cells/mL (MCF-7)	[56]
MGT-ABs-CuPc	Synergistic effect of enrichment from a porous TiO <sub>2</sub> shell and CT enhancement	HCC38 MDA-MB-231 MCF-7	5 × 10 <sup>2</sup> –5 × 10 <sup>5</sup> cells 5 × 10 <sup>2</sup> –10 <sup>6</sup> cells 5 × 10 <sup>3</sup> –5 × 10 <sup>4</sup> cells	3 cells / /	[104]
3D ZnO quantum	Synergistic effect of SPR effect and CT enhancement	MDAMB231 HeLa NIH3T3	/	/	[105]
Graphene	Synergistic effect of CT enhancement and π-π interaction between probe and graphene	Hemoglobin albumin	/	/	[107]
Quantum-size TiO <sub>2-x</sub>	Synergistic effect of effective enrichment of substrate and laser-induced CT resonances	ATP EGFR	/	/	[108]

Table 3. Cont.

SERS Substrate	Enhancement Mechanism	Target	Linear Range	LOD	Ref
Ni-MoS <sub>2</sub> NFs	Synergistic effect of effective enrichment of substrate and CT enhancement as well as interface dipole-dipole interaction	Bilirubin	10 <sup>-7</sup> –10 <sup>-3</sup> M	10 <sup>-7</sup> M	[109]
SnS <sub>2</sub> microspheres	Synergistic effect of the molecular enrichment caused by capillary effect and CT enhancement	SARS-CoV-2 S protein, SARS-CoV S protein, SARS-CoV-2 RNA	10 <sup>-14</sup> –10 <sup>-6</sup> M 10 <sup>4</sup> –10 <sup>7</sup> copies/mL 10 <sup>4</sup> –10 <sup>6</sup> copies/mL	10 <sup>-14</sup> M 10 <sup>7</sup> copies/mL 10 <sup>6</sup> copies/mL	[46]
Ta <sub>2</sub> C	Synergistic effect of PICT resonance enhancement and EM	SARS-CoV-2 S protein	/	5 × 10 <sup>-9</sup> M	[15]
1T'-MoTe <sub>2</sub>	CT enhancement	β-sitosterol	10 <sup>-9</sup> –10 <sup>-4</sup> M	10 <sup>-9</sup> M	[47]
Few-layered HfTe <sub>2</sub>	CT enhancement	Uric acid	100 μM–1 mM	100 μM	[117]
D-MIL-125-NH <sub>2</sub>	Photo-induced oxygen vacancy detection in D-MIL-125-NH <sub>2</sub> results in modified energy bands to boost both the inter-valence CT within MOFs and interfacial CT transitions	Dopamine	6.6 × 10 <sup>-4</sup> –6.6 × 10 <sup>-7</sup> M	6.6 × 10 <sup>-7</sup> M	[118]

## 5. Conclusions and Prospects

Non-noble metal nanomaterials have become the most promising SERS substrates due to their unique physicochemical properties. Although significantly fewer studies have been focused on their practical application compared with noble metals-based SERS substrates, they have shown their own advantages in addressing the challenges related to conventional SERS substrates and expanding the scope of SERS detection. In this review, we briefly summarized the enhancement mechanism of non-noble metal SERS substrates. Several main types of materials were also briefly reviewed. The latest application progress of non-noble metal materials based on SERS technology for the detection of pollutants and biomarkers in recent years is highlighted and discussed in detail. Although many innovative works have been completed, non-noble metal SERS substrates are still facing many limitations and require perpetual efforts in SERS detection. The following three aspects should be considered for the design of non-noble metal SERS substrates.

- (1) The lower detection sensitivity of most non-noble metal SERS substrates compared to noble metal SERS substrates (Au and Ag) is the main limiting factor for their applications. Therefore, the development of non-noble metal SERS substrates with high sensitivity can be made possible through the ability to rationally tune the multi-parametric combination of resonance conditions for the target;
- (2) The enhancement mechanism of non-noble metal SERS substrates is still needed to fully understand. Although more and more non-noble metal nanomaterials have been proposed, their enhancement mechanisms are different due to their various nanostructure and physicochemical properties. So far, the understanding of enhancement mechanisms is far from enough. In order to accurately control the SERS enhancement of non-noble metal nanomaterials, it is important to systematically research the enhancement mechanism of various non-noble metal nanomaterials;
- (3) In complex environments, background interference caused various characteristic peaks in the SERS spectrum, resulting in difficult-to-distinguish characteristic peaks of analytes. In addition to the specific recognition strategies of binding antigens and antibodies as well as aptamers to improve the selectivity of detection, various functionalized SERS tags that have aroused widespread interest in SERS anti-interference detection may alleviate this dilemma.



Although there is still a certain gap between the detection of non-noble metal SERS substrates in the lab and practical application, the development of novel SERS-active non-noble metal nanomaterials are meaningful to enrich the development of high-performance SERS substrates and to expand the practical application range of SERS. Especially given the development of detection strips, microfluidic chips, and kits based on non-noble metal nanomaterials combined with portable Raman may be a focus of future research. In addition, non-noble metal SERS active materials with good biocompatibility, low biotoxicity, and good spectral stability have also been proven to have imaging functions. This not only provides a new strategy for the development of a SERS platform for tumor diagnosis but also expands the application of SERS platforms based on non-noble metal nanomaterials in the accurate diagnosis and treatment of cancer. We believe and expect that with the development of related research, non-noble metal materials will eventually become the next generation of multifunctional SERS substrates for overcoming various challenges in practical applications.

**Funding:** This research was funded by the National Natural Science Foundation of China (No. 22074162), the Guangdong Provincial Natural Science Foundation of China (No. 2022A1515011171), and the State Key Program of National Natural Science of China (No. 22134007), respectively.

**Conflicts of Interest:** The authors declare no conflict of interest.

## References

1. Ji, W.; Zhao, B.; Ozaki, Y. Semiconductor Materials in Analytical Applications of Surface-Enhanced Raman Scattering. *J. Raman Spectrosc.* **2016**, *47*, 51–58. [[CrossRef](#)]
2. Pillai, I.C.L.; Li, S.; Romay, M.; Lam, L.; Lu, Y.; Huang, J.; Dillard, N.; Zemanova, M.; Rubbi, L.; Wang, Y. Cardiac Fibroblasts Adopt Osteogenic Fates and Can Be Targeted to Attenuate Pathological Heart Calcification. *Cell Stem Cell* **2017**, *20*, 218–232. [[CrossRef](#)] [[PubMed](#)]
3. Qian, X.M.; Nie, S.M. Single-Molecule and Single-Nanoparticle SERS: From Fundamental Mechanisms to Biomedical Applications. *Chem. Soc. Rev.* **2008**, *37*, 912–920. [[CrossRef](#)]
4. Xia, M. A Review on Applications of Two-Dimensional Materials in Surface-Enhanced Raman Spectroscopy. *Int. J. Spectrosc.* **2018**, *2018*, 4861472. [[CrossRef](#)]
5. Park, M.; Hwang, C.S.H.; Jeong, K.H. Nanoplasmonic Alloy of Au/Ag Nanocomposites on Paper Substrate for Biosensing Applications. *ACS Appl. Mater. Interfaces* **2018**, *10*, 290–295. [[CrossRef](#)] [[PubMed](#)]
6. Chang, R.; Wang, T.; Liu, Q.; Tang, J.; Wu, D. Ag Nanoparticles@Agar Gel as a 3D Flexible and Stable SERS Substrate with Ultrahigh Sensitivity. *Langmuir* **2022**, *38*, 13822–13832. [[CrossRef](#)]
7. Yang, B.; Jin, S.; Guo, S.; Park, Y.; Chen, L.; Zhao, B.; Jung, Y.M. Recent Development of SERS Technology: Semiconductor-Based Study. *ACS Omega* **2019**, *4*, 20101–20108. [[CrossRef](#)]
8. Lan, L.L.; Gao, Y.M.; Fan, X.C.; Li, M.Z.; Hao, Q.; Qiu, T. The Origin of Ultrasensitive SERS Sensing Beyond Plasmonics. *Front. Phys.* **2021**, *16*, 43300. [[CrossRef](#)]
9. Yin, Z.; Xu, K.; Jiang, S.; Luo, D.; Chen, R.; Xu, C.; Shum, P.; Liu, Y.J. Recent Progress on Two-Dimensional Layered Materials for Surface Enhanced Raman Spectroscopy and Their Applications. *Mater. Today Phys.* **2021**, *18*, 100378. [[CrossRef](#)]
10. Wang, X.J.; Zhang, E.J.; Shi, H.M.; Tao, Y.F.; Ren, X.D. Semiconductor-Based Surface Enhanced Raman Scattering (SERS): From Active Materials to Performance Improvement. *Analyst* **2022**, *147*, 1257–1272. [[CrossRef](#)]
11. Liu, Y.; Ma, H.; Han, X.X.; Zhao, B. Metal-Semiconductor Heterostructures for Surface-Enhanced Raman Scattering: Synergistic Contribution of Plasmons and Charge Transfer. *Mater. Horiz.* **2021**, *8*, 370–382. [[CrossRef](#)] [[PubMed](#)]
12. Alessandri, I.; Lombardi, J.R. Enhanced Raman Scattering with Dielectrics. *Chem. Rev.* **2016**, *116*, 14921–14981. [[CrossRef](#)] [[PubMed](#)]
13. Zhou, X.; Zhao, X.; Gu, S.; Gao, K.; Xie, F.; Wang, X.; Tang, Z. A Novel Sensitive ACNTs-MoO<sub>2</sub> SERS Substrate Boosted by Synergistic Enhancement Effect. *Phys. Chem. Chem. Phys.* **2021**, *23*, 20645–20653. [[CrossRef](#)]
14. Ye, Y.; Yi, W.; Liu, W.; Zhou, Y.; Bai, H.; Li, J.; Xi, G. Remarkable Surface-Enhanced Raman Scattering of Highly Crystalline Monolayer Ti<sub>3</sub>C<sub>2</sub> Nanosheets. *Sci. China Mater.* **2020**, *63*, 794–805. [[CrossRef](#)]
15. Peng, Y.; Lin, C.; Long, L.; Masaki, T.; Tang, M.; Yang, L.; Liu, J.; Huang, Z.; Li, Z.; Luo, X. Charge-Transfer Resonance and Electromagnetic Enhancement Synergistically Enabling MXenes with Excellent SERS Sensitivity for SARS-CoV-2 S Protein Detection. *Nano-Micro Lett.* **2021**, *13*, 52. [[CrossRef](#)] [[PubMed](#)]

16. Jiang, J.; Liu, H.; Li, X.; Chen, Y.; Gu, C.; Wei, G.; Zhou, J.; Jiang, T. Nonmetallic SERS-Based Immunosensor by Integrating MoS<sub>2</sub> Nanoflower and Nanosheet Towards the Direct Serum Detection of Carbohydrate Antigen 19-9. *Biosens. Bioelectron.* **2021**, *193*, 113481. [[CrossRef](#)] [[PubMed](#)]
17. Zhang, Y.; Zheng, B.; Zhu, C.; Zhang, X.; Tan, C.; Li, H.; Chen, B.; Yang, J.; Chen, J.; Huang, Y. Single-Layer Transition Metal Dichalcogenide Nanosheet-Based Nanosensors for Rapid, Sensitive, and Multiplexed Detection of DNA. *Adv. Mater.* **2015**, *27*, 935–939. [[CrossRef](#)]
18. Wang, X.; She, G.; Xu, H.; Mu, L.; Shi, W. The Surface-Enhanced Raman Scattering from ZnO Nanorod Arrays and its Application for Chemosensors. *Sens. Actuator B Chem.* **2014**, *193*, 745–751. [[CrossRef](#)]
19. Yu, J.; Lin, J.; Chen, M.; Meng, X.; Qiu, L.; Wu, J.; Xi, G.; Wang, X. Amorphous Ni(OH)<sub>2</sub> Nanocages as Efficient SERS Substrates for Selective Recognition in Mixtures. *Colloid Surf. A* **2021**, *631*, 127652. [[CrossRef](#)]
20. Zhang, J.; Xing, T.; Zhang, M.; Zhou, Y. Facile Preparation of Cu<sub>2-x</sub>S Supernanoparticles with an Unambiguous SERS Enhancement Mechanism. *Chem. Eng. J.* **2022**, *434*, 134457. [[CrossRef](#)]
21. Karthick Kannan, P.; Shankar, P.; Blackman, C.; Chung, C.H. Recent Advances in 2D Inorganic Nanomaterials for SERS Sensing. *Adv. Mater.* **2019**, *31*, e1803432. [[CrossRef](#)]
22. Liu, J.; He, H.; Xiao, D.; Yin, S.; Ji, W.; Jiang, S.; Luo, D.; Wang, B.; Liu, Y. Recent Advances of Plasmonic Nanoparticles and their Applications. *Materials* **2018**, *11*, 1833. [[CrossRef](#)] [[PubMed](#)]
23. Guerrini, L.; Graham, D. Molecularly-Mediated Assemblies of Plasmonic Nanoparticles for Surface-Enhanced Raman Spectroscopy Applications. *Chem. Soc. Rev.* **2012**, *41*, 7085–7107. [[CrossRef](#)] [[PubMed](#)]
24. Lombardi, J.R.; Birke, R.L. Theory of Surface-Enhanced Raman Scattering in Semiconductors. *J. Phys. Chem. C* **2014**, *118*, 11120–11130. [[CrossRef](#)]
25. Han, X.X.; Ji, W.; Zhao, B.; Ozaki, Y. Semiconductor-Enhanced Raman Scattering: Active Nanomaterials and Applications. *Nanoscale* **2017**, *9*, 4847–4861. [[CrossRef](#)]
26. Ji, W.; Li, L.; Song, W.; Wang, X.; Zhao, B.; Ozaki, Y. Enhanced Raman Scattering by ZnO Superstructures: Synergistic Effect of Charge Transfer and Mie Resonances. *Angew. Chem. Int. Ed.* **2019**, *58*, 14452–14456. [[CrossRef](#)] [[PubMed](#)]
27. Demirel, G.; Usta, H.; Yilmaz, M.; Celik, M.; Alidagi, H.A.; Buyukserin, F. Surface-Enhanced Raman spectroscopy (SERS): An Adventure from Plasmonic Metals to Organic Semiconductors as SERS Platforms. *J. Mater. Chem. C* **2018**, *6*, 5314–5335. [[CrossRef](#)]
28. Zheng, X.; Wu, X.; Zhang, L.; Kang, J.; Zhou, M.; Zhong, Y.; Zhang, J.; Wang, L. High Spin Fe<sup>3+</sup>-Related Bonding Strength and Electron Transfer for Sensitive and Stable SERS Detection. *Chem. Sci.* **2022**, *13*, 12560–12566. [[CrossRef](#)]
29. Wang, X.; Shi, W.; She, G.; Mu, L. Using Si and Ge Nanostructures as Substrates for Surface-Enhanced Raman Scattering Based on Photoinduced Charge Transfer Mechanism. *J. Am. Chem. Soc.* **2011**, *133*, 16518–16523. [[CrossRef](#)]
30. Yang, L.; Peng, Y.; Yang, Y.; Liu, J.; Huang, H.; Yu, B.; Zhao, J.; Lu, Y.; Huang, Z.; Li, Z. A Novel Ultra-Sensitive Semiconductor SERS Substrate Boosted by the Coupled Resonance Effect. *Adv. Sci.* **2019**, *6*, 1900310. [[CrossRef](#)]
31. Liang, X.; Li, N.; Zhang, R.; Yin, P.; Zhang, C.; Yang, N.; Liang, K.; Kong, B. Carbon-Based SERS Biosensor: From Substrate Design to Sensing and Bioapplication. *NPG Asia Mater.* **2021**, *13*, 8. [[CrossRef](#)]
32. Chen, M.; Liu, D.; Du, X.; Lo, K.H.; Wang, S.; Zhou, B.; Pan, H. 2D Materials: Excellent Substrates for Surface-Enhanced Raman Scattering (SERS) in Chemical Sensing and Biosensing. *TrAC-Trends Anal. Chem.* **2020**, *130*, 115983. [[CrossRef](#)]
33. Ling, X.; Xie, L.; Fang, Y.; Xu, H.; Zhang, H.; Kong, J.; Dresselhaus, M.S.; Zhang, J.; Liu, Z. Can Graphene Be Used as a Substrate for Raman Enhancement? *Nano Lett.* **2010**, *10*, 553–561. [[CrossRef](#)] [[PubMed](#)]
34. Feng, S.; Santos, M.C.D.; Carvalho, B.R.; Lv, R.; Li, Q.; Fujisawa, K.; Elías, A.L.; Lei, Y.; Perea-López, N.; Endo, M.; et al. Ultrasensitive Molecular Sensor Using N-Doped Graphene through Enhanced Raman Scattering. *Sci. Adv.* **2016**, *2*, e1600322. [[CrossRef](#)]
35. Ghopry, S.A.; Alamri, M.A.; Goul, R.; Sakidja, R.; Wu, J.Z. Extraordinary Sensitivity of Surface-Enhanced Raman Spectroscopy of Molecules on MoS<sub>2</sub> (WS<sub>2</sub>) Nanodomes/Graphene Van Der Waals Heterostructure Substrates. *Adv. Opt. Mater.* **2019**, *7*, 1801249. [[CrossRef](#)]
36. Singh, N.S.; Mayanglambam, F.; Nemade, H.B.; Giri, P.K. Facile Synthetic Route to Exfoliate High Quality and Super-Large Lateral Size Graphene-Based Sheets and Their Applications in SERS and CO<sub>2</sub> Gas Sensing. *RSC Adv.* **2021**, *11*, 9488–9504. [[CrossRef](#)]
37. Khan, K.; Tareen, A.K.; Aslam, M.; Wang, R.; Zhang, Y.; Mahmood, A.; Ouyang, Z.; Zhang, H.; Guo, Z. Recent Developments in Emerging Two-Dimensional Materials and Their Applications. *J. Mater. Chem. C* **2020**, *8*, 387–440. [[CrossRef](#)]
38. Zhou, J.; Yang, T.; Chen, J.; Wang, C.; Zhang, H.; Shao, Y. Two-Dimensional Nanomaterial-Based Plasmonic Sensing Applications: Advances and Challenges. *Coord. Chem. Rev.* **2020**, *410*, 213218. [[CrossRef](#)]
39. Ling, X.; Fang, W.; Lee, Y.H.; Araujo, P.T.; Zhang, X.; Rodriguez-Nieva, J.F.; Lin, Y.; Zhang, J.; Kong, J.; Dresselhaus, M.S. Raman Enhancement Effect on Two-Dimensional Layered Materials: Graphene, h-BN and MoS<sub>2</sub>. *Nano Lett.* **2014**, *14*, 3033–3040. [[CrossRef](#)]
40. Lee, Y.; Kim, H.; Lee, J.; Yu, S.H.; Hwang, E.; Lee, C.; Ahn, J.H.; Cho, J.H. Enhanced Raman Scattering of Rhodamine 6G Films on Two-Dimensional Transition Metal Dichalcogenides Correlated to Photoinduced Charge Transfer. *Chem. Mater.* **2015**, *28*, 180–187. [[CrossRef](#)]
41. Li, X.; Guo, S.; Su, J.; Ren, X.; Fang, Z. Efficient Raman Enhancement in Molybdenum Disulfide by Tuning the Interlayer Spacing. *ACS Appl. Mater. Interfaces* **2020**, *12*, 28474–28483. [[CrossRef](#)] [[PubMed](#)]

42. Majee, B.P.; Srivastava, V.; Mishra, A.K. Surface-Enhanced Raman Scattering Detection Based on an Interconnected Network of Vertically Oriented Semiconducting Few-Layer MoS<sub>2</sub> Nanosheets. *ACS Appl. Nano Mater.* **2020**, *3*, 4851–4858. [[CrossRef](#)]
43. Zuo, P.; Jiang, L.; Li, X.; Ran, P.; Li, B.; Song, A.; Tian, M.; Ma, T.; Guo, B.; Qu, L. Enhancing Charge Transfer with Foreign Molecules through Femtosecond Laser Induced MoS<sub>2</sub> Defect Sites for Photoluminescence Control and SERS Enhancement. *Nanoscale* **2019**, *11*, 485–494. [[CrossRef](#)] [[PubMed](#)]
44. Su, R.; Yang, S.; Han, D.; Hu, M.; Liu, Y.; Yang, J.; Gao, M. Ni and O Co-Modified MoS<sub>2</sub> as Universal SERS Substrate for the Detection of Different Kinds of Substances. *J. Colloid Interface Sci.* **2023**, *635*, 1–11. [[CrossRef](#)]
45. Li, M.; Fan, X.; Gao, Y.; Qiu, T. W<sub>18</sub>O<sub>49</sub>/Monolayer MoS<sub>2</sub> Heterojunction-Enhanced Raman Scattering. *J. Phys. Chem. Lett.* **2019**, *10*, 4038–4044. [[CrossRef](#)]
46. Peng, Y.; Lin, C.; Li, Y.; Gao, Y.; Wang, J.; He, J.; Huang, Z.; Liu, J.; Luo, X.; Yang, Y. Identifying Infectiousness of SARS-CoV-2 by Ultra-Sensitive SnS<sub>2</sub> SERS Biosensors with Capillary Effect. *Matter* **2022**, *5*, 694–709. [[CrossRef](#)]
47. Fraser, J.P.; Postnikov, P.; Miliutina, E.; Kolska, Z.; Valiev, R.; Svorcik, V.; Lyutakov, O.; Ganin, A.Y.; Guselnikova, O. Application of a 2D Molybdenum Telluride in SERS Detection of Biorelevant Molecules. *ACS Appl. Mater. Interfaces* **2020**, *12*, 47774–47783. [[CrossRef](#)]
48. Wang, K.; Guo, Z.; Li, Y.; Guo, Y.; Liu, H.; Zhang, W.; Zou, Z.; Zhang, Y.; Liu, Z. Few-Layer NbTe<sub>2</sub> Nanosheets as Substrates for Surface-Enhanced Raman Scattering Analysis. *ACS Appl. Nano Mater.* **2020**, *3*, 11363–11371. [[CrossRef](#)]
49. Samriti; Rajput, V.; Gupta, R.K.; Prakash, J. Engineering Metal Oxide Semiconductor Nanostructures for Enhanced Charge Transfer: Fundamentals and Emerging SERS Applications. *J. Mater. Chem. C* **2022**, *10*, 73–95. [[CrossRef](#)]
50. Yamada, H.; Yamamoto, Y.; Tan, N. Surface-Enhanced Raman Scattering (SERS) of Adsorbed Molecules on Smooth Surfaces of Metals and a Metal Oxide. *Chem. Phys. Lett.* **1982**, *86*, 397–400. [[CrossRef](#)]
51. Yamada, H.; Yamamoto, Y. Surface Enhanced Raman Scattering (SERS) of Chemisorbed Species on Various Kinds of Metals and Semiconductors. *Surf. Sci.* **1983**, *134*, 71–90. [[CrossRef](#)]
52. Chen, J.; Sun, K.; Zhang, Y.; Wu, D.; Jin, Z.; Xie, F.; Zhao, X.; Wang, X. Plasmonic MoO<sub>2</sub> Nanospheres Assembled on Graphene Oxide for Highly Sensitive SERS Detection of Organic Pollutants. *Anal. Bioanal. Chem.* **2019**, *411*, 2781–2791. [[CrossRef](#)] [[PubMed](#)]
53. Wu, H.; Zhou, X.; Li, J.; Li, X.; Li, B.; Fei, W.; Zhou, J.; Yin, J.; Guo, W. Ultrathin Molybdenum Dioxide Nanosheets as Uniform and Reusable Surface-Enhanced Raman Spectroscopy Substrates with High Sensitivity. *Small* **2018**, *14*, e1802276. [[CrossRef](#)]
54. Miao, P.; Wu, J.; Du, Y.; Sun, Y.; Xu, P. Phase Transition Induced Raman Enhancement on Vanadium Dioxide (VO<sub>2</sub>) nanosheets. *J. Mater. Chem. C* **2018**, *6*, 10855–10860. [[CrossRef](#)]
55. Li, Y.; Bai, H.; Zhai, J.; Yi, W.; Li, J.; Yang, H.; Xi, G. Alternative to Noble Metal Substrates: Metallic and Plasmonic Ti<sub>3</sub>O<sub>5</sub> Hierarchical Microspheres for Surface Enhanced Raman Spectroscopy. *Anal. Chem.* **2019**, *91*, 4496–4503. [[CrossRef](#)]
56. Lin, J.; Ren, W.; Li, A.; Yao, C.; Chen, T.; Ma, X.; Wang, X.; Wu, A. Crystal-Amorphous Core-Shell Structure Synergistically Enabling TiO<sub>2</sub> Nanoparticles' Remarkable SERS Sensitivity for Cancer Cell Imaging. *ACS Appl. Mater. Interfaces* **2020**, *12*, 4204–4211. [[CrossRef](#)]
57. Zheng, X.; Zhong, H.; Wang, Z.; Li, J.; Hu, Y.; Li, H.; Jia, J.; Zhang, S.; Ren, F. Fabrication of Stable Substoichiometric WO<sub>x</sub> Films with High SERS Sensitivity by Thermal Treatment. *Vacuum* **2022**, *198*, 110884. [[CrossRef](#)]
58. Zhong, X.; Sun, Y.; Chen, X.; Zhuang, G.; Li, X.; Wang, J.G. Mo Doping Induced More Active Sites in Urchin-Like W<sub>18</sub>O<sub>49</sub> Nanostructure with Remarkably Enhanced Performance for Hydrogen Evolution Reaction. *Adv. Funct. Mater.* **2016**, *26*, 5778–5786. [[CrossRef](#)]
59. Xie, X.; Gao, N.; Huang, Y.; Fang, Y. SERS Monitored Kinetic Process of Gaseous Thiophenol Compound in Plasmonic MOF Nanoparticles. *ACS Appl. Mater. Interfaces* **2022**, *14*, 51468–51475. [[CrossRef](#)]
60. Zhang, Y.; Xue, C.; Xu, Y.; Cui, S.; Ganeev, A.A.; Kistenev, Y.V.; Gubal, A.; Chuchina, V.; Jin, H.; Cui, D. Metal-Organic Frameworks Based Surface-Enhanced Raman Spectroscopy Technique for Ultra-Sensitive Biomedical Trace Detection. *Nano Res.* **2023**, *16*, 2968–2979. [[CrossRef](#)]
61. Meng, J.; Liu, X.; Niu, C.; Pang, Q.; Li, J.; Liu, F.; Liu, Z.; Mai, L. Advances in Metal-Organic Framework Coatings: Versatile Synthesis and Broad Applications. *Chem. Soc. Rev.* **2020**, *49*, 3142–3186. [[CrossRef](#)] [[PubMed](#)]
62. Sugikawa, K.; Nagata, S.; Furukawa, Y.; Kokado, K.; Sada, K. Stable and Functional Gold Nanorod Composites with a Metal-Organic Framework Crystalline Shell. *Chem. Mater.* **2013**, *25*, 2565–2570. [[CrossRef](#)]
63. He, L.; Liu, Y.; Liu, J.; Xiong, Y.; Zheng, J.; Liu, Y.; Tang, Z. Core-Shell Noble-Metal@Metal-Organic-Framework Nanoparticles with Highly Selective Sensing Property. *Angew. Chem. Int. Ed.* **2013**, *52*, 3741–3745. [[CrossRef](#)]
64. Hu, Y.; Liao, J.; Wang, D.; Li, G. Fabrication of Gold Nanoparticle-Embedded Metal-Organic Framework for Highly Sensitive Surface-Enhanced Raman Scattering Detection. *Anal. Chem.* **2014**, *86*, 3955–3963. [[CrossRef](#)] [[PubMed](#)]
65. Yu, T.H.; Ho, C.H.; Wu, C.Y.; Chien, C.H.; Lin, C.H.; Lee, S. Metal-Organic Frameworks: A Novel SERS Substrate. *J. Raman Spectrosc.* **2013**, *44*, 1506–1511. [[CrossRef](#)]
66. Sun, H.; Cong, S.; Zheng, Z.; Wang, Z.; Chen, Z.; Zhao, Z. Metal-Organic Frameworks as Surface Enhanced Raman Scattering Substrates with High Tailorability. *J. Am. Chem. Soc.* **2019**, *141*, 870–878. [[CrossRef](#)]
67. Fu, J.H.; Zhong, Z.; Xie, D.; Guo, Y.J.; Kong, D.X.; Zhao, Z.X.; Zhao, Z.X.; Li, M. SERS-Active MIL-100(Fe) Sensory Array for Ultrasensitive and Multiplex Detection of VOCs. *Angew. Chem. Int. Ed.* **2020**, *59*, 20489–20498. [[CrossRef](#)]

68. Zheng, T.; Zhou, Y.; Feng, E.; Tian, Y. Surface-enhanced Raman Scattering on 2D Nanomaterials: Recent Developments and Applications. *Chin. J. Chem.* **2021**, *39*, 745–756. [[CrossRef](#)]
69. Sarycheva, A.; Makaryan, T.; Maleski, K.; Satheeshkumar, E.; Melikyan, A.; Minassian, H.; Yoshimura, M.; Gogotsi, Y. Two-Dimensional Titanium Carbide (MXene) as Surface-Enhanced Raman Scattering Substrate. *J. Phys. Chem. C* **2017**, *121*, 19983–19988. [[CrossRef](#)]
70. Soundiraraju, B.; George, B.K. Two-Dimensional Titanium Nitride (Ti<sub>2</sub>N) MXene: Synthesis, Characterization, and Potential Application as Surface-Enhanced Raman Scattering Substrate. *ACS Nano* **2017**, *11*, 8892–8900. [[CrossRef](#)]
71. Yang, K.; Zhu, K.; Wang, Y.; Qian, Z.; Zhang, Y.; Yang, Z.; Wang, Z.; Wu, L.; Zong, S.; Cui, Y. Ti<sub>3</sub>C<sub>2</sub>T<sub>x</sub> MXene-Loaded 3D Substrate toward On-Chip Multi-Gas Sensing with Surface-Enhanced Raman Spectroscopy (SERS) Barcode Readout. *ACS Nano* **2021**, *15*, 12996–13006. [[CrossRef](#)] [[PubMed](#)]
72. Malik, A.H.; Habib, F.; Qazi, M.J.; Ganayee, M.A.; Ahmad, Z.; Yattoo, M.A. A Short Review Article on Conjugated Polymers. *J. Polym. Res.* **2023**, *30*, 115. [[CrossRef](#)]
73. Yang, Z.; Ma, C.; Gu, J.; Wu, Y.; Zhu, C.; Li, L.; Gao, H.; Yin, W.; Wang, Z.; Zhang, Y. SERS Detection of Benzoic Acid in Milk by Using Ag-COF SERS Substrate. *Spectrochim. Acta A Mol. Biomol. Spectrosc.* **2022**, *267*, 120534. [[CrossRef](#)] [[PubMed](#)]
74. Liu, Q.; Zhang, R.; Yu, B.; Liang, A.; Jiang, Z. A Highly Sensitive Gold Nanosol SERS Aptamer Assay for Glyphosate with a New COF Nanocatalytic Reaction of Glycol-Au (III). *Sens. Actuator B Chem.* **2021**, *344*, 130288. [[CrossRef](#)]
75. Chen, J.; Liu, C.; Hu, D.; Wang, F.; Wu, H.; Gong, X.; Liu, X.; Song, L.; Sheng, Z.; Zheng, H. Single-Layer MoS<sub>2</sub> Nanosheets with Amplified Photoacoustic Effect for Highly Sensitive Photoacoustic Imaging of Orthotopic Brain Tumors. *Adv. Funct. Mater.* **2016**, *26*, 8715–8725. [[CrossRef](#)]
76. Lin, C.; Liang, S.; Peng, Y.; Long, L.; Li, Y.; Huang, Z.; Long, N.V.; Luo, X.; Liu, J.; Li, Z. Visualized SERS Imaging of Single Molecule by Ag/Black Phosphorus Nanosheets. *Nano-Micro Lett.* **2022**, *14*, 75. [[CrossRef](#)]
77. Liu, Z.; Chen, H.; Jia, Y.; Zhang, W.; Zhao, H.; Fan, W.; Zhang, W.; Zhong, H.; Ni, Y.; Guo, Z. A Two-Dimensional Fingerprint Nanoprobe Based on Black Phosphorus for Bio-SERS Analysis and Chemo-Photothermal Therapy. *Nanoscale* **2018**, *10*, 18795–18804. [[CrossRef](#)]
78. Barhoumi, A.; Halas, N.J. Label-Free Detection of DNA Hybridization Using Surface Enhanced Raman Spectroscopy. *J. Am. Chem. Soc.* **2010**, *132*, 12792–12793. [[CrossRef](#)]
79. Wu, D.; Chen, J.; Ruan, Y.; Sun, K.; Zhang, K.; Xie, W.; Xie, F.; Zhao, X.; Wang, X. A Novel Sensitive and Stable Surface Enhanced Raman Scattering Substrate Based on a MoS<sub>2</sub> Quantum Dot/Reduced Graphene Oxide Hybrid System. *J. Mater. Chem. C* **2018**, *6*, 12547–12554. [[CrossRef](#)]
80. Park, J.; Thomasson, J.A.; Gale, C.C.; Sword, G.A.; Lee, K.M.; Herrman, T.J.; Suh, C.P. Adsorbent-SERS Technique for Determination of Plant VOCs from Live Cotton Plants and Dried Teas. *ACS Omega* **2020**, *5*, 2779–2790. [[CrossRef](#)]
81. Maharjan, S.; Yun, Y.J.; Okello, V.A.; Wiederrecht, G.P.; Gosztola, D.J.; Ayitou, A.J.L. Photometric Sensing of Heavy Metal Ions Using a Naphthoquinodimethyl-Bis-Thioamide Dye: Selectivity & Photophysics of the Metal Organic Complexes. *J. Photochem. Photobiol. A* **2022**, *424*, 113648.
82. Kamal, S.; Yang, T.C. Silver Enriched Silver Phosphate Microcubes as an Efficient Recyclable SERS Substrate for the Detection of Heavy Metal ions. *J. Colloid Interface Sci.* **2022**, *605*, 173–181. [[CrossRef](#)]
83. Zhang, H.; Huang, S.; Yang, X.; Yuan, R.; Chai, Y. A SERS Biosensor Constructed by Calcined ZnO Substrate with High-Efficiency Charge Transfer for Sensitive Detection of Pb<sup>2+</sup>. *Sens. Actuator B Chem.* **2021**, *343*, 130142. [[CrossRef](#)]
84. Parveen, S.; Saifi, S.; Akram, S.; Husain, M.; Zulfequar, M. ZnO Nanoparticles Functionalized SWCNTs as Highly Sensitive SERS Substrate for Heavy Metal Ions Detection. *Mater. Sci. Semicond. Process.* **2022**, *149*, 106852. [[CrossRef](#)]
85. Ji, W.; Wang, Y.; Tanabe, I.; Han, X.; Zhao, B.; Ozaki, Y. Semiconductor-Driven “Turn-Off” Surface-Enhanced Raman Scattering Spectroscopy: Application in Selective Determination of Chromium (VI) in Water. *Chem. Sci.* **2015**, *6*, 342–348. [[CrossRef](#)] [[PubMed](#)]
86. Xie, Z.; Feng, Y.; Wang, F.; Chen, D.; Zhang, Q.; Zeng, Y.; Lv, W.; Liu, G. Construction of Carbon Dots Modified MoO<sub>3</sub>/g-C<sub>3</sub>N<sub>4</sub> Z-Scheme Photocatalyst with Enhanced Visible-Light Photocatalytic Activity for the Degradation of Tetracycline. *Appl. Catal. B Environ.* **2018**, *229*, 96–104. [[CrossRef](#)]
87. Qu, L.L.; Liu, Y.Y.; Liu, M.K.; Yang, G.H.; Li, D.W.; Li, H.T. Highly Reproducible Ag NPs/CNT-Intercalated GO Membranes for Enrichment and SERS Detection of Antibiotics. *ACS Appl. Mater. Interfaces* **2016**, *8*, 28180–28186. [[CrossRef](#)]
88. Singh, J.; Rishikesh; Kumar, S.; Soni, R.K. Synthesis of 3D-MoS<sub>2</sub> Nanoflowers with Tunable Surface Area for the Application in Photocatalysis and SERS Based Sensing. *J. Alloys Compd.* **2020**, *849*, 156502. [[CrossRef](#)]
89. Zhang, Q.; Li, X.; Yi, W.; Li, W.; Bai, H.; Liu, J.; Xi, G. Plasmonic MoO<sub>2</sub> Nanospheres as a Highly Sensitive and Stable Non-Noble Metal Substrate for Multicomponent Surface-Enhanced Raman Analysis. *Anal. Chem.* **2017**, *89*, 11765–11771. [[CrossRef](#)]
90. Liang, P.; Cao, Y.; Dong, Q.; Wang, D.; Zhang, D.; Jin, S.; Yu, Z.; Ye, J.; Zou, M. A Balsam Pear-Shaped CuO SERS Substrate with Highly Chemical Enhancement for Pesticide Residue Detection. *Mikrochim. Acta* **2020**, *187*, 335. [[CrossRef](#)]



91. Quan, Y.; Su, R.; Yang, S.; Chen, L.; Wei, M.; Liu, H.; Yang, J.; Gao, M.; Li, B. In-Situ Surface-Enhanced Raman Scattering Based on MTi<sub>20</sub> Nanoflowers: Monitoring and Degradation of Contaminants. *J. Hazard. Mater.* **2021**, *412*, 125209. [[CrossRef](#)] [[PubMed](#)]
92. Gokulakrishnan; Alex, K.V.; Sekhar, K.C.; Koppole, K. Highly Sensitive, Cost-Effective, and Flexible SERS Substrate Based on Green Synthesized GO/rGO for Pesticide Detection. *ChemistrySelect* **2022**, *7*, e202200348.
93. Guo, C.; Sun, J.; Dong, J.; Cai, W.; Zhao, X.; Song, B.; Zhang, R. A Natural Anthocyanin-Based Multifunctional Theranostic Agent for Dual-Modal Imaging and Photothermal Anti-Tumor Therapy. *J. Mater. Chem. B* **2021**, *9*, 7447–7460. [[CrossRef](#)] [[PubMed](#)]
94. Shao, H.; Lin, H.; Guo, Z.; Lu, J.; Jia, Y.; Ye, M.; Su, F.; Niu, L.; Kang, W.; Wang, S. A Multiple Signal Amplification Sandwich-Type SERS Biosensor for Femtomolar Detection of MiRNA. *Biosens. Bioelectron.* **2019**, *143*, 111616. [[CrossRef](#)]
95. Liu, X.; Zhou, Y.; Zheng, T.; Tian, Y. Surface-Enhanced Raman Scattering Technology Based on WO<sub>3</sub> Film for Detection of VEGF. *Chem. Res. Chin. Univ.* **2021**, *37*, 900–905. [[CrossRef](#)]
96. Atlas, G. Editorial: The 16th Annual Nucleic Acids Research Web Server Issue 2018. *Nucleic Acids Res.* **2018**, *46*, W1–W4.
97. Brancati, G.; Grosshans, H. An Interplay of MiRNA Abundance and Target Site Architecture Determines MiRNA Activity and Specificity. *Nucleic Acids Res.* **2018**, *46*, 3259–3269. [[CrossRef](#)]
98. Jiang, L.; Hu, Y.; Zhang, H.; Luo, X.; Yuan, R.; Yang, X. Charge-Transfer Resonance and Surface Defect-Dominated WO<sub>3</sub> Hollow Microspheres as SERS Substrates for the MiRNA 155 Assay. *Anal. Chem.* **2022**, *94*, 6967–6975. [[CrossRef](#)]
99. Liu, J.; Zheng, T.; Tian, Y. Functionalized h-BN Nanosheets as a Theranostic Platform for SERS Real-Time Monitoring of MicroRNA and Photodynamic Therapy. *Angew. Chem. Int. Ed.* **2019**, *58*, 7757–7761. [[CrossRef](#)]
100. Yu, L.; Ng, S.R.; Xu, Y.; Dong, H.; Wang, Y.J.; Li, C.M. Advances of Lab-on-a-Chip in Isolation, Detection and Post-Processing of Circulating Tumour Cells. *Lab Chip* **2013**, *13*, 3163–3182. [[CrossRef](#)] [[PubMed](#)]
101. Feng, Z.; Wu, J.; Lu, Y.; Chan, Y.T.; Zhang, C.; Wang, D.; Luo, D.; Huang, Y.; Feng, Y.; Wang, N. Circulating Tumor Cells in the Early Detection of Human Cancers. *Int. J. Biol. Sci.* **2022**, *18*, 3251–3265. [[CrossRef](#)] [[PubMed](#)]
102. Xu, Y.; Lin, J.; Wu, X.; Xu, X.; Zhang, D.; Xie, Y.; Pan, T.; He, Y.; Wu, A.; Shao, G. A TiO<sub>2</sub>-Based Bioprobe Enabling Excellent SERS Activity in the Detection of Diverse Circulating Tumor Cells. *J. Mater. Chem. B* **2022**, *10*, 3808–3816. [[CrossRef](#)] [[PubMed](#)]
103. Xu, X.; Lin, J.; Guo, Y.; Wu, X.; Xu, Y.; Zhang, D.; Zhang, X.; Yujiao, X.; Wang, J.; Yao, C. TiO<sub>2</sub>-Based Surface-Enhanced Raman Scattering Bio-Probe for Efficient Circulating Tumor Cell Detection on Microfilter. *Biosens. Bioelectron.* **2022**, *210*, 114305. [[CrossRef](#)] [[PubMed](#)]
104. Feng, E.; Zheng, T.T.; He, X.X.; Chen, J.Q.; Tian, Y. A Novel Ternary Heterostructure with Dramatic SERS Activity for Evaluation of PD-L1 Expression at the Single-Cell Level. *Sci. Adv.* **2018**, *4*, eaau3494. [[CrossRef](#)]
105. Haldavnekar, R.; Venkatakrishnan, K.; Tan, B. Non Plasmonic Semiconductor Quantum SERS Probe as a Pathway for in Vitro Cancer Detection. *Nat. Commun.* **2018**, *9*, 3065. [[CrossRef](#)]
106. Wang, Z.; Zong, S.; Wu, L.; Zhu, D.; Cui, Y. SERS-Activated Platforms for Immunoassay: Probes, Encoding Methods, and Applications. *Chem. Rev.* **2017**, *117*, 7910–7963. [[CrossRef](#)]
107. Huang, S.; Pandey, R.; Barman, I.; Kong, J.; Dresselhaus, M. Raman Enhancement of Blood Constituent Proteins Using Graphene. *ACS Photonics* **2018**, *5*, 2978–2982. [[CrossRef](#)]
108. Dharmalingam, P.; Venkatakrishnan, K.; Tan, B. An Atomic-Defect Enhanced Raman scattering (DERS) Quantum Probe for Molecular Level Detection-Breaking the SERS Barrier. *Appl. Mater. Today* **2019**, *16*, 28–41. [[CrossRef](#)]
109. Su, R.; Quan, Y.; Yang, S.; Hu, M.; Yang, J.; Gao, M. Destroying the Symmetric Structure to Promote Phase Transition: Improving the SERS Performance and Catalytic Activity of MoS<sub>2</sub> Nanoflowers. *J. Alloys Compd.* **2021**, *886*, 161268. [[CrossRef](#)]
110. Tang, Z.; Kong, N.; Zhang, X.; Liu, Y.; Hu, P.; Mou, S.; Liljeström, P.; Shi, J.; Tan, W.; Kim, J.S. A Materials-Science Perspective on Tackling COVID-19. *Nat. Rev. Mater.* **2020**, *5*, 847–860. [[CrossRef](#)]
111. Jiang, Y.; Hu, M.; Liu, A.A.; Lin, Y.; Liu, L.; Yu, B.; Zhou, X.; Pang, D.W. Detection of SARS-CoV-2 by CRISPR/Cas12a-Enhanced Colorimetry. *ACS Sens.* **2021**, *6*, 1086–1093. [[CrossRef](#)]
112. Li, Y.; Chen, H.; Guo, Y.; Wang, K.; Zhang, Y.; Lan, P.; Guo, J.; Zhang, W.; Zhong, H.; Guo, Z. Lamellar Hafnium Ditetelluride as an Ultrasensitive Surface-Enhanced Raman Scattering Platform for Label-Free Detection of Uric Acid. *Photonics Res.* **2021**, *9*, 1039–1047. [[CrossRef](#)]
113. Sun, H.; Song, G.; Gong, W.; Lu, W.; Cong, S.; Zhao, Z. Stabilizing Photo-Induced Vacancy Defects in MOF Matrix for High-Performance SERS Detection. *Nano Res.* **2022**, *15*, 5347–5354. [[CrossRef](#)]
114. Ferná'ndez, R.D.; Ruth, T.J.; Sossi, V.; Schulzer, M.; Calne, D.B.; Stoessl, A.J. Expectation and Dopamine Release: Mechanism of the Placebo Effect in Parkinson's Disease. *Science* **2001**, *293*, 1164–1166. [[CrossRef](#)] [[PubMed](#)]
115. Zhang, A.; Neumeyer, J.L.; Baldessarini, R.J. Recent Progress in Development of Dopamine Receptor Subtype-Selective Agents: Potential Therapeutics for Neurological and Psychiatric Disorders. *Chem. Rev.* **2007**, *107*, 274–302. [[CrossRef](#)] [[PubMed](#)]
116. Shim, J.E.; Kim, Y.J.; Choe, J.H.; Lee, T.G.; You, E.A. Single-Nanoparticle-Based Digital SERS Sensing Platform for the Accurate Quantitative Detection of SARS-CoV-2. *ACS Appl. Mater. Interfaces* **2022**, *14*, 38459–38470. [[CrossRef](#)]
117. Wu, P.; Luo, X.; Xu, Y.; Zhu, J.; Jia, W.; Fang, N.; Cai, C.; Zhu, J.J. Long-Range SERS Detection of the SARS-CoV-2 Antigen on a Well-Ordered Gold Hexagonal Nanoplate Film. *Anal. Chem.* **2022**, *94*, 17541–17550. [[CrossRef](#)]
118. Yue, W.; Xia, Z.; Zeng, Z.; Chen, Z.; Qiao, L.; Li, P.; He, Y.; Luo, X. In Situ Surface-Enhanced Raman Scattering Detection of a SARS-CoV-2 Biomarker Using Flexible and Transparent Polydimethylsiloxane Films with Embedded Au Nanoplates. *ACS Appl. Nano Mater.* **2022**, *5*, 12897–12906. [[CrossRef](#)]

119. Hwang, C.S.H.; Lee, S.; Lee, S.; Kim, H.; Kang, T.; Lee, D.; Jeong, K.H. Highly Adsorptive Au-TiO<sub>2</sub> Nanocomposites for the SERS Face Mask Allow the Machine-Learning-Based Quantitative Assay of SARS-CoV-2 in Artificial Breath Aerosols. *ACS Appl. Mater. Interfaces* **2022**, *14*, 54550–54557. [[CrossRef](#)]
120. Zhao, T.; Liang, P.; Ren, J.; Zhu, J.; Yang, X.; Bian, H.; Li, J.; Cui, X.; Fu, C.; Xing, J. Gold-Silver Alloy Hollow Nanoshells-Based Lateral Flow Immunoassay for Colorimetric, Photothermal, and SERS Tri-Mode Detection of SARS-CoV-2 Neutralizing Antibody. *Anal. Chim. Acta* **2023**, *1255*, 341102. [[CrossRef](#)] [[PubMed](#)]

**Disclaimer/Publisher's Note:** The statements, opinions and data contained in all publications are solely those of the individual author(s) and contributor(s) and not of MDPI and/or the editor(s). MDPI and/or the editor(s) disclaim responsibility for any injury to people or property resulting from any ideas, methods, instructions or products referred to in the content.